THE FIRST SYSTEMATIC STUDY OF TYPE Ibc SUPERNOVA MULTI-BAND LIGHT CURVES

MARIA R. DROUT[1,2], ALICIA M. SODERBERG[1], AVISHAY GAL-YAM[3], S. BRADLEY CENKO[4], DEREK B. FOX[5],
DOUGLAS C. LEONARD[6], DAVID J. SAND[7,8], DAE-SIK MOON[9], IAIR ARCAVI[3], AND YOAV GREEN[3]

[1] Harvard-Smithsonian Center for Astrophysics, Cambridge, MA 02138, USA
[2] Churchill College, Cambridge CB3 0DS, UK
[3] Benoziyo Center for Astrophysics, Faculty of Physics, The Weizmann Institute of Science, Rehovot 76100, Israel
[4] Department of Astronomy, University of California, Berkeley, CA 94720-3411, USA
[5] Department of Astronomy and Astrophysics, Pennsylvania State University, University Park, PA 16802, USA
[6] Department of Astronomy, San Diego State University, San Diego, CA 92182, USA
[7] Las Cumbres Observatory Global Telescope Network, Santa Barbara, CA 93117, USA
[8] Department of Physics, University of California, Santa Barbara, CA 93106, USA
[9] Department of Astronomy and Astrophysics, University of Toronto, Toronto, ON M5S 3H4, Canada

ABSTRACT

We present detailed optical photometry for 25 Type Ibc supernovae (SNe Ibc) within $d \approx 150$ Mpc obtained with the robotic Palomar 60 inch telescope in 2004–2007. This study represents the first uniform, systematic, and statistical sample of multi-band SNe Ibc light curves available to date. We correct the light curves for host galaxy extinction using a new technique based on the photometric color evolution, namely, we show that the $(V - R)$ color of extinction-corrected SNe Ibc at $\Delta t \approx 10$ days after V-band maximum is tightly distributed, $\langle (V - R)_{V10} \rangle = 0.26 \pm 0.06$ mag. Using this technique, we find that SNe Ibc typically suffer from significant host galaxy extinction, $\langle E(B - V) \rangle \approx 0.4$ mag. A comparison of the extinction-corrected light curves for helium-rich (Type Ib) and helium-poor (Type Ic) SNe reveals that they are statistically indistinguishable, both in luminosity and decline rate. We report peak absolute magnitudes of $\langle M_R \rangle = -17.9 \pm 0.9$ mag and $\langle M_R \rangle = -18.3 \pm 0.6$ mag for SNe Ib and Ic, respectively. Focusing on the broad-lined (BL) SNe Ic, we find that they are more luminous than the normal SNe Ibc sample, $\langle M_R \rangle = -19.0 \pm 1.1$ mag, with a probability of only 1.6% that they are drawn from the same population of explosions. By comparing the peak absolute magnitudes of SNe Ic-BL with those inferred for local engine-driven explosions (GRB-SN 1998bw, XRF-SN 2006aj, and SN 2009bb) we find a 25% probability that relativistic SNe are drawn from the overall SNe Ic-BL population. Finally, we fit analytic models to the light curves to derive typical ^{56}Ni masses of $M_{Ni} \approx 0.2$ and $0.5 \, M_\odot$ for SNe Ibc and SNe Ic-BL, respectively. With reasonable assumptions for the photospheric velocities, we further extract kinetic energy and ejecta mass values of $M_{ej} \approx 2 \, M_\odot$ and $E_K \approx 10^{51}$ erg for SNe Ibc, while for SNe Ic-BL we find higher values, $M_{ej} \approx 5 \, M_\odot$ and $E_K \approx 10^{52}$ erg. We discuss the implications for the progenitors of SNe Ibc and their relation to those of engine-driven explosions.

Key words: supernovae: general – gamma-ray burst: general

Online-only material: color figures, machine-readable table

1. INTRODUCTION

Type Ibc supernovae (SNe Ibc) are a distinct class of catastrophic stellar explosions, identified by the lack of hydrogen features and the presence of weak silicon features in their optical spectra (see Filippenko 1997 for a review). In the traditional classification scheme, the presence and strength of helium absorption features *may* further differentiate the class of SNe Ibc into two sub-classes: Ib (He-rich) and Ic (He-poor; see Matheson et al. 2001). Based on their proximity to star-forming regions (Porter & Filippenko 1987; van Dyk et al. 1996), and their often strong radio/X-ray emission attributed to circumstellar interaction (Weiler et al. 1986; Chevalier 1998; Berger et al. 2003; Chevalier & Fransson 2006; Soderberg 2007), SNe Ibc are now recognized as core-collapse explosions of massive stars[10] stripped of their hydrogen (and often helium) layers (Elias et al. 1985; Filippenko & Sargent 1985; Wheeler & Levreault 1985; Uomoto & Kirshner 1985; Clocchiatti et al. 1996; Woosley et al. 2002).

Unlike other core-collapse SNe, however, the progenitor systems of SNe Ibc have yet to be directly identified in pre-explosion images (see Smartt 2009 for a review). Motivated by their observed properties, two primary progenitor channels have been proposed: (1) isolated and massive Wolf-Rayet (WR) stars that ejected their outer envelope through radiation-driven stellar winds (Begelman & Sarazin 1986; Woosley et al. 1995), and (2) lower mass helium stars in close binary systems characterized by mass transfer (Wheeler & Levreault 1985; Podsiadlowski et al. 1992; Yoon et al. 2010). It remains open to debate whether one or both of these progenitor channels gives rise to the observed SN Ibc population.

Recent host galaxy studies suggest dissimilar progenitor channels for SNe Ib and Ic based on the properties (e.g., luminosity, chemistry, and star-formation rate) of the explosion sites (Kelly et al. 2008; Prieto et al. 2008; Arcavi et al. 2010; Modjaz et al. 2011 but see Anderson et al. 2010). These results indicate that progenitor age, mass, and/or metallicity drive the observed optical spectroscopic diversity seen for SNe Ibc, namely the presence/strength of the He I features. Furthermore, the discovery that some SNe Ic produce relativistic outflows that give rise to long-duration gamma-ray bursts (GRBs) points to a unique progenitor channel for a small fraction of these

---

[10] There are notable exceptions, however, which comprise only a small fraction of the bulk SN Ibc population and include SN 2005E-like white dwarf events (Perets et al. 2010), pair-instability SNe (Gal-Yam et al. 2009), and pulsational pair-instability SNe (Quimby et al. 2011).

events (see Woosley & Bloom 2006 for a review). These relativistic outflows are powered by an additional energy source, a central engine, commonly thought to be a rapidly rotating and accreting compact object (MacFadyen et al. 2001) or a magnetar (Thompson et al. 2004). We refer to these explosions as "engine-driven."

In this paper, we search for additional progenitor clues based on the optical light curves of SNe Ibc. Free from the massive envelopes and/or circumstellar shells associated with other core-collapse explosions, the photospheric emission of "naked" SNe Ibc is powered by the radioactive decay of freshly synthesized ^{56}Ni. This optical signal reaches maximum intensity within a month of the explosion, producing parabola-shaped light curves that resemble those of SNe Ia. In the simple picture, three physical parameters determine the shape of the light curves and peak luminosity: the mass of newly synthesized ^{56}Ni ($M_{\rm Ni}$), the total ejecta mass ($M_{\rm ej}$), and the kinetic energy of the explosion (E_K; see Arnett 1982). In addition, spectroscopic measurements of the photospheric velocity, $v_{\rm ph}$, directly constrain the quantity, $\sqrt{E_K/M_{\rm ej}}$. Since the explosion parameters are imprinted on the optical emission, their detailed study can reveal clues as to the properties and diversity within the progenitor channel(s).

Literature studies of the photospheric emission from SNe Ibc are relatively few (Richardson et al. 2006) and tend to focus on detailed photometric and/or spectroscopic observations of single explosions. These studies often target those SNe Ibc with extreme properties, such as the 5%–10% of the population showing evidence for unusually broad absorption features ("broad-lined," BL; Podsiadlowski et al. 2004) and photospheric velocities of $v_{\rm ph} \gtrsim 20,000\,{\rm km\,s^{-1}}$ (e.g., SN 2003jd; Valenti et al. 2008). Such events are spectroscopically similar to GRB-SNe. Preliminary comparisons of the optical luminosities of ordinary SNe Ibc and GRB-SNe revealed overlap between the two samples, with GRB-SNe populating the upper end of the SN luminosity distribution (Soderberg et al. 2006a; Woosley & Bloom 2006; Richardson 2009). However, a more comprehensive and uniform sample of ordinary SNe Ibc is required for a robust comparison.

More recently, a set of two dozen unfiltered light curves for SNe Ibc was reported by the Lick Observatory Supernova Search (LOSS) within an estimated completeness limit of $d \approx 60$ Mpc (Li et al. 2011). The LOSS light curves reveal an overall dispersion in decay rate and peak magnitude with some evidence that SNe Ib are more luminous than SNe Ic. However, due to the lack of photometric color information and often poor light curve coverage of the LOSS SNe Ibc, a robust and systematic study of their multi-band light curves and host galaxy extinction-corrected peak luminosities, and an extraction of their explosion parameters remain outstanding projects.

Motivated thus, between 2004 and 2007 we conducted a dedicated optical monitoring campaign of nearby SNe Ibc with the robotic Palomar 60 inch telescope (P60; Cenko et al. 2006). The primary goal of this effort was to observationally constrain the physical parameters of the explosion ($M_{\rm Ni}$, $M_{\rm ej}$, and E_K). In this paper, we present the P60 light curves for a sample of 25 SNe Ibc, representing the first uniform and systematic multi-band study to date. We present a novel approach to correcting the light curves for (often significant) host galaxy extinction. We compare the observed light curve properties with those of SNe Ibc compiled from the literature and engine-driven SNe within the same volume, and we derive the physical parameters for the extended sample using a systematic modeling approach. The

parameters are compared for SNe Ib, Ic, and SNe Ic-BL with the goal of shedding light on the progenitor channels. Finally, we provide our SNe Ibc light curves and light curve templates to the community to facilitate ongoing and future efforts to distinguish between SNe Ia and SN Ibc at larger distances and/or without spectroscopic diagnostics.

2. OBSERVATIONS AND PHOTOMETRY

We used the robotic Palomar 60 inch telescope (P60; Cenko et al. 2006) to obtain multi-epoch, multi-band optical observations for our SN follow-up campaign. P60 is a queue-scheduled facility dedicated to rapid-response and monitoring observations of optical transients. We selected targets for our study from the sample of local ($d \lesssim 150$ Mpc) SN discoveries publicly announced via the online circulars, including the International Astronomical Union Circulars (IAUC), Central Bureau for Electronic Telegrams (CBET), and the Astronomers Telegram (ATEL) between Fall 2004 and Spring 2007. We note that the majority of these SNe were discovered by SN searches that target the most luminous (and likely metal-rich) nearby galaxies (e.g., LOSS).

Here we present the P60 data from our campaign for all 25 SNe spectroscopically classified and reported in the online circulars as Type Ib (11 events), Ic (11 events), and Ic-BL (three events) for which we were able to obtain at least eight photometric measurements. We note that two SNe Ib in our sample subsequently developed hydrogen features prompting their re-classification as Type IIb and we include them here given their connection to the Type Ib class (e.g., Chevalier & Soderberg 2010).

The majority of the SNe in this sample (15 of the 25) were observed between Fall 2005 and Spring 2007 (see Soderberg 2007). An additional 10 SNe were observed as part of the Caltech Core-Collapse supernova Program (CCCP; Gal-Yam et al. 2007), which carried out photometric and spectroscopic follow-up of all young ($\lesssim$30 days since explosion) and nearby ($d \lesssim 120$ Mpc) SNe of Types Ibc or II between 2004 July and 2005 September. We note that the CCCP data for the peculiar, Ca-rich SN 2005E were reported separately by Perets et al. (2010) and so we do not include them here.

The properties of each SN in our sample are summarized in Table 1, including spectroscopic classification, host galaxy distance, and Galactic extinction (Schlegel et al. 1998). For SNe with conflicting classification reports, we adopt the latest classification since He I absorption features often become more prominent with age (e.g., SN 1999ex; Hamuy et al. 2002). We adopt host galaxy distances from the NASA/IPAC Extragalactic Database of cosmology independent distances (NED-D[11]) when available. For the remaining objects we adopt the NED distances after correction for Virgo, Great Attractor, and Shapley Supercluster Infall and assuming $H_0 = 73$ km s^{-1} Mpc^{-1} (Mould et al. 2000).

For each newly discovered SN accessible to P60, we promptly initiated nightly photometric follow-up in the Johnson V and R bands. The sensitivity functions of these filters are described and displayed in Cenko et al. (2006). Our monitoring campaign was optimized for a cadence of ~1 day, with observations typically extending for several months after discovery. All P60 images were reduced in IRAF[12] using a custom real-time reduction

---

[11] http://nedwww.ipac.caltech.edu/Library/Distances/.
[12] IRAF is distributed by the National Optical Astronomy Observatory, which is operated by the Association for Research in Astronomy, Inc., under cooperative agreement with the National Science Foundation.

Table 1
Sample of SNe Ibc

SN	Host Galaxy	Distance (Mpc)	Inclination (deg)	$E(B-V)$ Galactic (mag)[a]	Discovery Circular[b]	Spectral Type	Classification Circular[b]
2004dk[c]	NGC 6118	23 ± 2[d]	$67^{+0.7}_{-0.7}$	0.157	I8377	Ib	I8404
2004dn[c]	UGC 2069	51 ± 4	56^{+3}_{-3}	0.048	I8381	Ic	I8381
2004fe[c]	NGC 132	72 ± 5	43^{+4}_{-5}	0.025	I8425	Ic	I8426
2004ff[c]	ESO 552-G40	92 ± 7	66^{+4}_{-5}	0.032	I8425	Ic	I8428
2004ge[c]	UGC 3555	67 ± 5	28^{+12}_{-28}	0.087	I8443	Ic	I8453
2004gk[c]	IC 3311	17 ± 1[d,e]	~ 90	0.030	I8446	Ic	I8446
2004gq[c]	NGC 1832	26 ± 6[d]	50^{+3}_{-4}	0.073	I8452	Ib	I8461
2004gt[c,f]	NGC 4038	23 ± 2	56^{+2}_{-2}	0.046	I8454	Ic	I8456
2004gv[c]	NGC 856	79 ± 6	46^{+6}_{-9}	0.033	I8454	Ib	I8456
2005az[c]	NGC 4961	39 ± 4[d]	47^{+4}_{-5}	0.011	I8503	Ib	A451
2005eo	UGC 4132	85 ± 7[d]	80^{+4}_{-4}	0.067	I8605	Ic	I8605
2005hg	UGC 1394	86 ± 6	60^{+3}_{-4}	0.105	I8623	Ib	C271
2005kz	MCG +08-34-32	115 ± 8	60^{+5}_{-7}	0.054	I8639	Ic-BL	I8639
2005la[g]	Anon.	76 ± 8[h]	. . .	0.011	I8639	IIb	I8639
2005mf	UGC 4798	113 ± 8	30^{+12}_{-30}	0.018	I8648	Ic	I8650
2005nb	UGC 7230	106 ± 7	55^{+4}_{-5}	0.037	I8657	Ic-BL	I8657
2006F	NGC 935	55 ± 4	53^{+5}_{-7}	0.190	I8658	Ib	I8660
2006ab	PGC 10652	68 ± 5	65^{+3}_{-4}	0.489	I8669	Ic	I8677
2006ck	UGC 8238	112 ± 11[d]	61^{+5}_{-7}	0.028	I8713	Ic	I8713
2006dn	UGC 12188	70 ± 7[h]	40^{+6}_{-9}	0.113	I8728	Ib	A854
2006el	UGC 12188	70 ± 7[h]	40^{+6}_{-9}	0.113	I8741	IIb	C626
2006fo	UGC 2019	82 ± 6	34^{+12}_{-34}	0.029	I8570	Ic	I8770
2006jc[i]	UGC 4904	28 ± 2	59^{+4}_{-5}	0.020	I8762	Ibn	C677
2007C	NGC 4981	25 ± 3[d]	43^{+3}_{-3}	0.042	I8792	Ib	I8792
2007D	UGC 2653	93 ± 7	70^{+4}_{-6}	0.335	I8794	Ic-BL	C805

Notes.

[a] Milky Way extinction estimates adopted from Schlegel et al. (1998).

[b] Entries refer to electronic circular numbers prefaced by "I" (IAUC), "C" (CBET), or "A" (ATEL), and the full references are listed below.

[c] P60 observations conducted under the Caltech Core-Collapse Supernova Program.

[d] Redshift-independent distance.

[e] Host galaxy is a member of the Virgo cluster. Distance is adopted from Mould et al. (2000).

[f] Previous photometry has been published by Gal-Yam et al. (2005).

[g] Previous photometry has been published by Pastorello et al. (2008b).

[h] Distance is derived from the host galaxy redshift reported in (Antilogus et al. 2006, ATel 854).

[i] Previous photometry has been published by Foley et al. (2007) and Pastorello et al. (2007).

[j] Distance is an average of the value reported in Saviane et al. (2004) and the Tully-Fisher distance referenced by LEDA.

References. (I8377) Graham & Li 2004a; (I8404) Filippenko et al. 2004; (I8381) Graham & Li 2004b; (I8425) Pugh et al. 2004; (I8426) Modjaz et al. 2004b; (I8428) Modjaz et al. 2004a; (I8443) Moore et al. 2004; (I8453) Filippenko & Foley 2004; (I8446) Quimby et al. 2004; (I8452) Pugh et al. 2004; (I8461) Modjaz et al. 2005d; (I8454) Monard et al. 2004; (I8456) Ganeshalingam et al. 2004; (I8503) Quimby et al. 2005; (A451) Aldering et al. 2005; (I8605) Puckett et al. 2005a; Modjaz et al. 2005a; (I8623) Shimasaki & Li 2005; (C271) Modjaz et al. 2005c; (I8639) Puckett et al. 2005b; Filippenko et al. 2005; (I8648) Newton & Puckett 2005; (I8650) Modjaz et al. 2005b; (I8657) Quimby et al. 2006; (I8658) Colesanti et al. 2006; (I8660) Baek et al. 2006; (I8669) Lee et al. 2006; (I8677) Wong et al. 2006; (I8713) Colesanti et al. 2006; (I8728) Schwehr & Li 2006; (A854) Antilogus et al. 2006; (I8741) Puckett et al. 2006b; (C626) Blondin et al. 2006; (I8570) Puckett et al. 2006a; (I8770) Prasad et al. 2006; (I8762) Itagaki et al. 2006; (C677) Modjaz et al. 2006; (I8792) Puckett et al. 2007; (I8794) Joubert et al. 2007; (C805) Foley & Gal-Yam 2007.

pipeline (Cenko et al. 2006). In Figure 1, we display a montage of the $1\rlap{.}'5 \times 1\rlap{.}'5$ region around each SN as observed with P60.

We used point-spread function (PSF) photometry to extract the relative magnitudes of the SNe with respect to several stars within the full $13' \times 13'$ P60 field of view.[13] Absolute calibration of the relative light curves was performed using a combination of P60 observations of Landolt standard fields and Sloan Digital Sky Survey (SDSS) photometry of field stars. We used the

Smith et al. (2002) transformations to convert the SDSS *ugriz* photometry of field stars to the V and R bands.

The P60 photometry for all 25 SNe is available in Table 2 (machine-readable) and are characterized by typical uncertainties of ~ 0.02 to 0.05 mag epoch^{-1}. We supplemented our photometry with measurements from the literature, primarily drawn from the initial discovery circulars, thereby providing early-time and often pre-discovery flux measurements including upper limits (see Table 1 for references). In this compilation, we have assumed that unfiltered magnitudes from the circulars are roughly equivalent to R-band measurements and assign to the detections an uncertainty of ± 0.2 mag. In cases where

---

[13] We compare our PSF photometry light curves for SNe 2004dk and 2004dn with those produced after digitally subtracting the host galaxy emission using the common PSF method and find them to be comparable (A. Gal-Yam et al. 2011, in preparation).
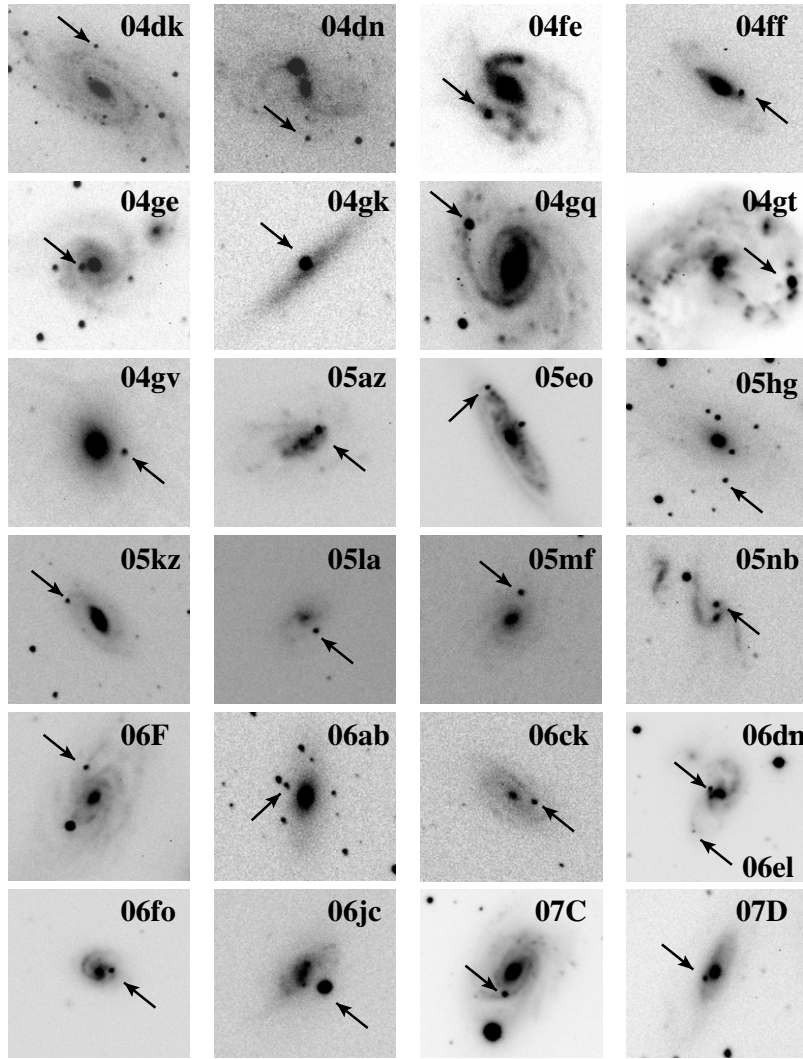
Figure 1. P60 images of 25 SNe Ibc in our study. Each stamp is 1.5 × 1.5 arcmin, north is up, and east is to the left. The SNe are marked by arrows.

Table 2
P60 Photometry

SN	Filter	JD	Magnitude
SN 2004dk	V	2453219.8	16.99 ± 0.03
. . .	. . .	2453220.7	16.69 ± 0.03
. . .	. . .	2453223.8	15.88 ± 0.02
. . .	. . .	2453233.7	14.74 ± 0.02
. . .	. . .	2453234.7	14.69 ± 0.02
. . .	. . .	2453237.8	14.55 ± 0.02
. . .	. . .	2453242.7	14.50 ± 0.02
. . .	. . .	2453252.6	14.72 ± 0.02
. . .	. . .	2453258.6	14.91 ± 0.03
. . .	. . .	2453261.6	15.01 ± 0.02
. . .	. . .	2453266.6	15.17 ± 0.02

(This table is available in its entirety in a machine-readable form in the online journal. A portion is shown here for guidance regarding its form and content.)

extensive photometry is available from the literature, we find that our photometry is fully consistent (i.e., SN 2006jc, Pastorello et al. 2007; SN 2005la, Pastorello et al. 2008b)

2.1. Sample Definitions

Our SN Ibc light curves can be divided into three groups, based on constraints on the epoch and apparent magnitude of the light curve maxima. For the eight SNe in the Gold group, our P60 observations covered the light curve maximum in both V and R bands (Figure 2). These data alone nearly double the existing sample of well-studied SNe Ibc light curves available in the literature. The Silver group is composed of nine SNe for which the R-band light curve maximum is observationally constrained through a combination of P60 monitoring and literature measurements (Figure 3). Finally, there are eight SNe in our Bronze group, for which the epoch and magnitude of the light curve maximum is poorly constrained in both bands (Figure 4). As shown in Figures 2–4, the light curve shapes are diverse.

3. OBSERVED LIGHT CURVE PROPERTIES

The shape of the SN Ibc light curves is fully determined by the three explosion parameters, E_K, M_{ej}, and M_{Ni} (e.g., Arnett 1982). Specifically, the peak optical luminosity, L_{peak}, scales with the mass of ^{56}Ni as $L_{peak} \propto M_{Ni} \tau_c^{-1}$. Here, $\tau_c \approx 8 M_{ej,\odot}^{3/4} E_{K,51}^{-1/4}$ days is the characteristic time or width of the light curve and our notation refers to a normalization of E_K by 10^{51} erg and of M_{ej} by $M_\odot$ (Iwamoto et al. 2003). Light curves with larger τ_c values have correspondingly slower post-maximum decay rates. Therefore, while L_{peak} is primarily determined by the fractional mass of ^{56}Ni, the width of the light curve (and, in turn, the decay
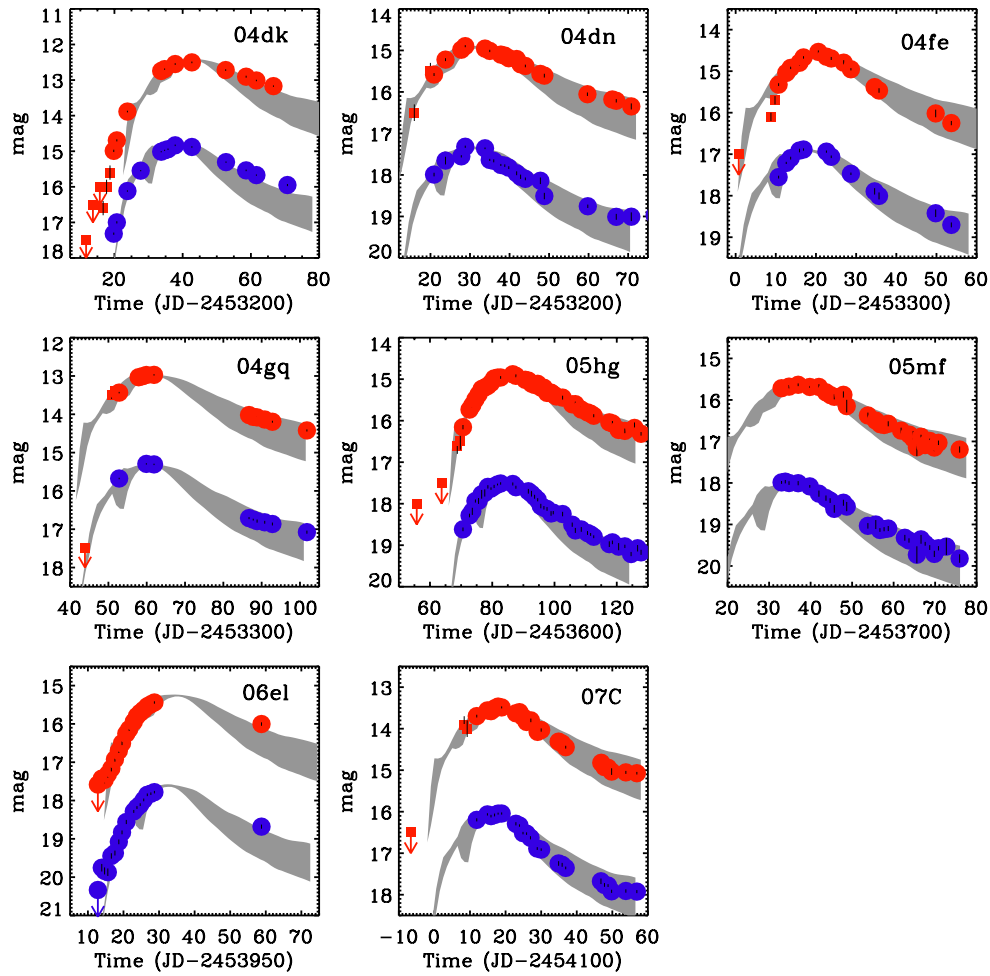
Figure 2. Apparent *V*-band (blue) and *R*-band (red) light curves for our Gold sample of SNe Ibc. This sample includes only those SNe for which our P60 data reveal the epoch and flux of maximum light in both bands. Circles designate P60 points and squares represent measurements drawn from the discovery circulars (see Table 1 for references). The *R*-band points have been brightened by 2 mag for clarity. We have made no corrections for extinction (Galactic or host galaxy). The gray curves are the template light curves constructed from the sample of literature SNe Ibc and overplotted for comparison (see Section 3.1 and Figure 5).

(A color version of this figure is available in the online journal.)

rate) is determined by M_{ej} and E_K. In our study of SNe Ibc light curves, we therefore focus on their two main observable properties, namely their peak absolute magnitudes and post-maximum decay rates. To enable a systematic comparison of these observables, we first define a procedure and apply it to an existing set of well-studied SNe Ibc available in the literature.

3.1. The Sample of Literature SNe

We compiled *V*- and *R*-band photometry for the existing sample of well-studied SNe Ibc within a similar distance of $d \lesssim 150$ Mpc that are available in the literature.[14] Our selection criteria required the light curve maxima to be well sampled and the total extinction to have been estimated using the equivalent width of the Na I D lines and/or fitting of the broadband photometric spectrum. After excluding the SNe associated with GRBs (SN 1998bw, Galama et al. 1998; SN 2006aj, Pian et al. 2006) and the notably peculiar events (i.e., the Ca-rich SN 2005E; Perets et al. 2010, the double-peaked SN 2005bf; Folatelli et al. 2006, and the SNe Ibn 2006jc and 2005la; Foley et al. 2007; Pastorello et al. 2007, 2008b), we construct a sample

of 10 SNe Ibc: 1994I, 1999ex, 2002ap, 2003jd, 2004aw, 2007Y, 2007gr, 2007ru, 2008D, and 2008ax. In Table 3, we compile the basic properties of this literature sample including the SN type, the Galactic extinction (from Schlegel et al. 1998), and the host galaxy name, distance estimate, and inclination. In line with the P60 sample, we adopt up-to-date NED-D host galaxy distances for the literature sample when available. In Table 4, we further list the epoch and apparent magnitude of the *V*- and *R*-band light curve maxima. For three of the literature SNe, the published light curves were obtained in the SDSS *r*-band filter, and we converted these to *R* band using the transformations of Smith et al. (2002). These are noted in Table 3. We note that more detailed transformations (e.g., S corrections; Stritzinger et al. 2002) are outside the scope of this paper, and thus the derived *R*-band photometry for these three SNe may include a small systematic uncertainty.

After correcting the light curves for the typically low Galactic extinction ($\langle E(B-V)_{Gal}\rangle \approx 0.06$ mag), we derive peak absolute magnitudes in the *V* and *R* bands and find that they span ~ 3–4 mag. This has been noted previously based on similar samples of SNe Ibc drawn from the literature (Richardson et al. 2006; Soderberg et al. 2006a). In the *R* band, the range extends from $M_{R,\text{peak}} \approx -15.6$ to -18.9 mag. Dividing the sample into SNe Ib, Ic, and Ic-BL (4, 3, and 3 SNe, respectively),

---

[14] We note that with these selection criteria, we exclude the rare, overluminous SNe Ibc detected in magnitude-limited surveys, e.g., SN 2007bi (Gal-Yam et al. 2009) and SN 2005ap (Quimby et al. 2011).
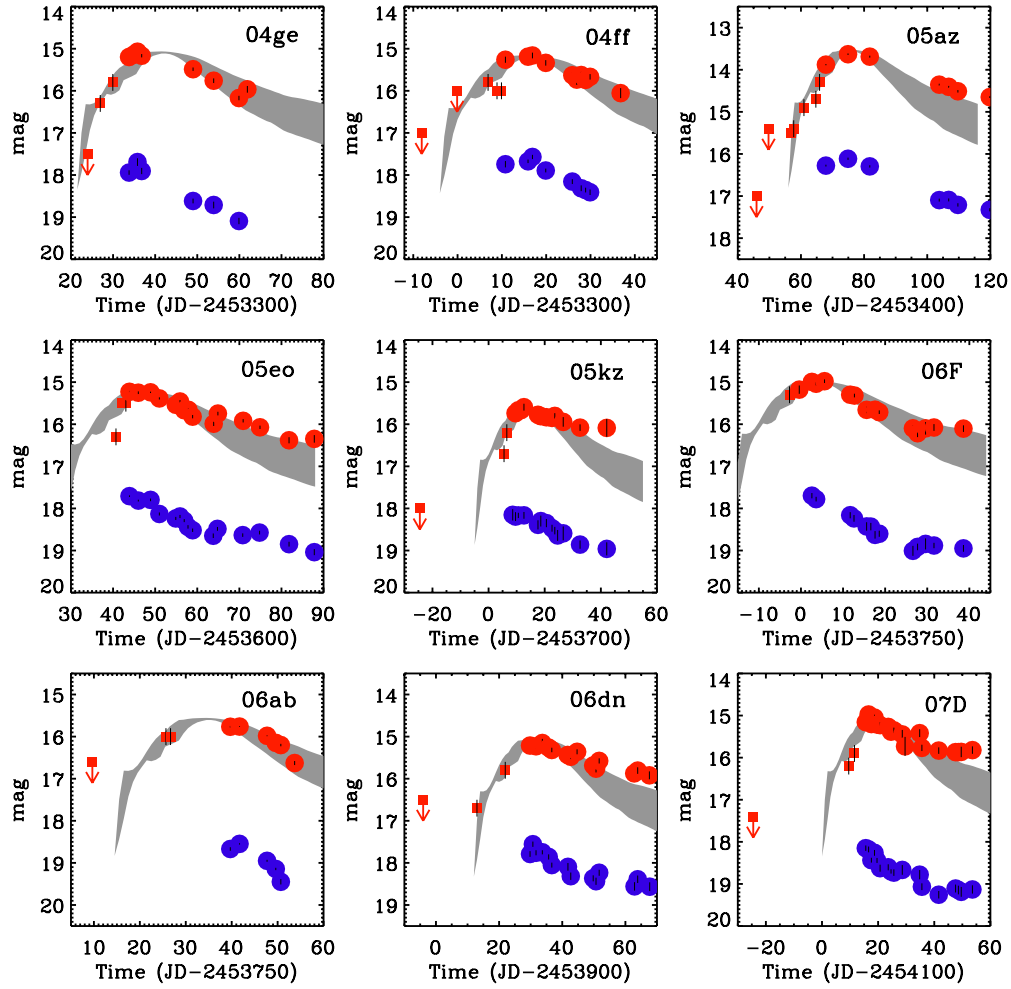
Figure 3. Apparent *V*-band (blue) and *R*-band (red) light curves for our Silver sample of SNe Ibc which includes SNe for which the epoch and flux of maximum light in the *R* band is well constrained by supplementing our P60 measurements with photometry from the literature. Circles designate P60 points and squares represent measurements adopted from the discovery circulars (see Table 1 for references). The *R*-band points have been brightened by 2 mag for clarity. We have made no corrections for extinction (Galactic or host galaxy). The gray curves are the template light curves constructed from the sample of literature SNe Ibc and overplotted for comparison (see Section 3.1 and Figure 5).

(A color version of this figure is available in the online journal.)

Table 3
Literature SNe Ibc Sample

SN	Host Galaxy	Distance (Mpc)	Inclination (deg)	$E(B-V)$ Galactic (mag)[a]	Spectral Type	Ref.
1994I	NGC 5194	7.1 ± 1.2[b]	53^{+1}_{-1}	0.035	Ic	1
1999ex	IC 5179	46 ± 4[c]	64^{+2}_{-3}	0.020	Ib	2
2002ap	NGC 628	8.2 ± 1.2[c]	25^{+3}_{-3}	0.071	Ic-BL	3
2003jd	MCG -01-59-21	77 ± 5	42^{+8}_{-14}	0.044	Ic-BL	4
2004aw	NGC 3997	73 ± 5	71^{+2}_{-2}	0.021	Ic	5
2007Y	NGC 1187	18 ± 2[c]	43^{+3}_{-3}	0.022	Ib	6
2007gr	NGC 1058	9.3 ± 0.7[d]	22^{+6}_{-10}	0.062	Ic	7
2007ru	UGC 12381	64 ± 5	31^{+10}_{-23}	0.259	Ic-BL	8
2008D	NGC 2770	30 ± 3[c]	77^{+1}_{-1}	0.023	Ib	9
2008ax	NGC 4490	8.7 ± 1.2[c]	63^{+1}_{-1}	0.022	IIb	10

Notes.
[a] Milky Way extinction estimates adopted from Schlegel et al. (1998).
[b] Distance is from Takáts & Vinkó (2006).
[c] Redshift-independent distance.
[d] Distance is from Silbermann et al. (1996).

References. (1) Richmond et al. 1996; (2) Stritzinger et al. 2002; (3) Foley et al. 2003; (4) Valenti et al. 2008; (5) Taubenberger et al. 2006; (6) Stritzinger et al. 2009; (7) Hunter et al. 2009; (8) Sahu et al. 2009; (9) Soderberg et al. 2008; (10) Pastorello et al. 2008a.
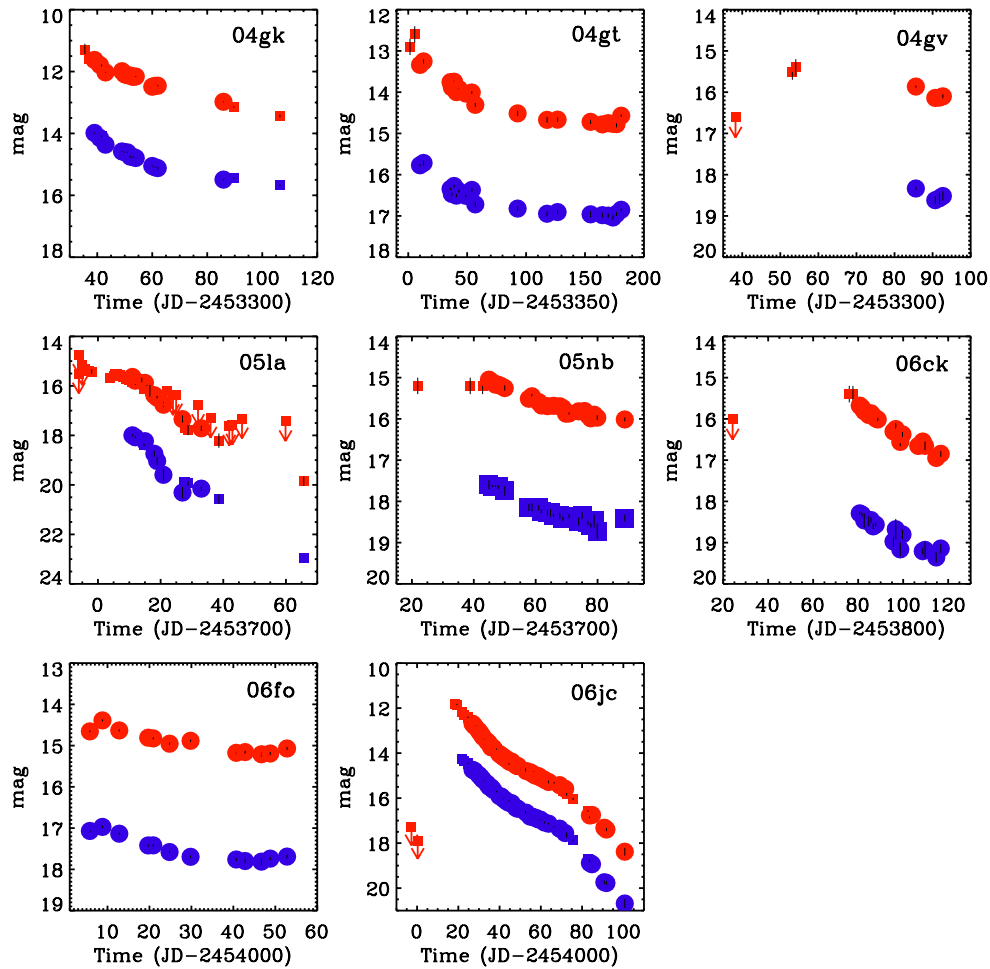
Figure 4. Apparent *V*-band (blue) and *R*-band (red) light curves for our Bronze sample of SNe Ibc which includes SNe for which the epoch and flux of maximum light are poorly constrained. Circles designate P60 points and squares represent measurements drawn from the literature including discovery circulars (see Table 1) and in the case of SNe 2005la and 2006jc, measurements were also drawn from Pastorello et al. (2008b) and Pastorello et al. (2007), respectively. The *R*-band points have been brightened by 2 mag for clarity. We have made no corrections for extinction (Galactic or host galaxy).

(A color version of this figure is available in the online journal.)

we calculate mean values of $\langle M_{R,\mathrm{peak}} \rangle = -16.3 \pm 0.6$ mag (Ib), $\langle M_{R,\mathrm{peak}} \rangle = -17.1 \pm 0.4$ mag (Ic), and $\langle M_{R,\mathrm{peak}} \rangle = -18.4 \pm 0.8$ mag (Ic-BL).

We next compare the light curve shapes of the literature sample after shifting each curve relative to the epoch and magnitude of maximum light (Figure 5). This figure highlights the significant dispersion in the light curve widths (see also Clocchiatti & Wheeler 1997a, Clocchiatti & Wheeler 1997b). We build template light curves in the *V* and *R* bands by interpolating over these normalized light curves and extracting the weighted mean flux density for time intervals spanning -20 to $+40$ days with respect to the epoch of maximum light. The uncertainties in the resulting templates are derived from the standard deviation in the interpolated curves at each time interval and represent the intrinsic dispersion in light curve widths. Our resulting template curves are shown in Figure 5.

We measure the post-maximum decay rate for each of the literature SNe using the Δm_{15} diagnostic which represents the decay in magnitudes during the 15 days following the light curve maximum (Phillips 1993). By interpolating over the well-sampled *V*- and *R*-band light curves, we derive $\Delta m_{15,V}$ and $\Delta m_{15,R}$ estimates, respectively (Table 4). We note that this is a variation on the standard definition for Δm_{15} which assumes a time baseline relative to the *B*-band light curve

maximum. As shown in Figure 6, the literature sample reveals a broad dispersion in Δm_{15} with mean values of $\langle \Delta m_{15,V} \rangle = 0.94 \pm 0.31$ mag and $\langle \Delta m_{15,R} \rangle = 0.74 \pm 0.27$ mag. Thus, the *R*-band light curves decay more slowly than the *V*-band ones.

After dividing the literature sample into the SN sub-classes, we find that the $\Delta m_{15,R}$ values are statistically consistent: $\langle \Delta m_{15,R} \rangle = 0.7 \pm 0.1$ mag (Ib), $\langle \Delta m_{15,R} \rangle = 0.9 \pm 0.5$ mag (Ic), and $\langle \Delta m_{15,R} \rangle = 0.7 \pm 0.1$ mag (Ic-BL). We also note that the fast-fading Type Ic SN 1994I is a 2σ outlier of the overall SN Ibc distribution.

3.2. The Sample of P60 SNe

Since the light curves for some of the SNe in our P60 sample are not as densely sampled as those of the literature sample, we use the $V-$ and R-band template light curves described above to fit the epoch and magnitude of the light curve maxima for all Gold and Silver P60 SNe. We use a χ^2 minimization technique for the template-fitting analysis and extract typical uncertainties on the epoch and apparent magnitude at maximum of about ± 0.5 (± 1.0) days and ± 0.1 (± 0.2) mag, respectively, for the Gold (Silver) SNe. For the Silver SNe, we fit only the *R*-band light curves since the *V*-band data are insufficient to estimate the parameters of the light curve maxima. The Gold and Silver P60 light curves are compared with the individual template

Table 4
Light Curve Properties of the Literature SNe Ibc

SN[a]	Band	Peak Time (JD)	Peak Apparent Magnitude	Δm_{15} (mag)	$E(B-V)$ Host (mag)[b]	$(V-R)_{10 \text{ days}}$ (mag)[c]	Peak Absolute Magnitude
1994I	V	2449451.44 ± 0.03	12.91 ± 0.02	1.67 ± 0.05	0.42	0.19	-17.94 ± 0.39
	R	2449451.92 ± 0.04	12.65 ± 0.02	1.40 ± 0.06	...	0.20	-17.65 ± 0.39
1999ex	V	2451501.2 ± 0.5	16.63 ± 0.04	0.96 ± 0.10	0.26	0.33	-17.53 ± 0.23
	R	2451502.7 ± 0.5	16.26 ± 0.02	0.81 ± 0.05	...	0.37	-17.68 ± 0.21
2002ap	V	2452313.42 ± 0.16	12.360 ± 0.006	0.90 ± 0.04	0.0	0.31	-17.43 ± 0.32
	R	2452315.74 ± 0.18	12.267 ± 0.003	0.69 ± 0.06	...	0.35	-17.50 ± 0.32
2003jd	V	2452944.1 ± 1.0	15.94 ± 0.18	0.97 ± 0.33	0.10	0.24	-18.93 ± 0.33
	R	2452944.7 ± 1.0	15.82 ± 0.15	0.74 ± 0.25	...	0.26	-18.94 ± 0.30
2004aw	V	2453091.1 ± 0.6	17.30 ± 0.03	0.59 ± 0.14	0.35	0.30	-18.16 ± 0.18
	R	2453095.0 ± 0.6	16.90 ± 0.03	0.39 ± 0.11	...	0.44	-18.27 ± 0.18
2007Y	V	2454165.6 ± 0.5	15.336 ± 0.011	1.07 ± 0.05	0.09	0.24	-16.29 ± 0.20
	R[d]	2454166.5 ± 0.5	15.322 ± 0.015	0.72 ± 0.05	...	0.25	-16.22 ± 0.21
2007gr	V	2454338.5 ± 1.1	12.91 ± 0.01	0.95 ± 0.11	0.03	0.34	-17.22 ± 0.17
	R	2454341.0 ± 1.7	12.76 ± 0.02	0.78 ± 0.13	...	0.31	-17.30 ± 0.18
2007ru	V	2454439.2 ± 0.5	15.95 ± 0.015	0.75 ± 0.07	0.01	0.22	-18.92 ± 0.17
	R	2454439.2 ± 0.5	15.68 ± 0.019	0.51 ± 0.07	...	0.22	-18.99 ± 0.17
2008D	V	2454491.7 ± 0.5	17.40 ± 0.02	0.55 ± 0.08	0.59	0.22	-16.91 ± 0.26
	R[d]	2454491.7 ± 0.5	16.84 ± 0.04	0.55 ± 0.13	...	0.30	-17.00 ± 0.28
2008ax	V	2454549.5 ± 0.5	13.51 ± 0.02	0.94 ± 0.05	0.28	0.22	-17.11 ± 0.33
	R[d]	2454341.0 ± 1.7	12.76 ± 0.02	0.78 ± 0.13	...	0.23	-17.05 ± 0.35

Notes.
[a] The total extinction estimates, peak times, and peak apparent magnitudes in the V and R bands were compiled from the following references: (1994I) Richmond et al. 1996; (1999ex) Stritzinger et al. 2002; (2002ap) Foley et al. 2003; (2003jd) Valenti et al. 2008; (2004aw) Taubenberger et al. 2006; (2007Y) Stritzinger et al. 2009; (2007gr) Hunter et al. 2009; (2007ru) Sahu et al. 2009; (2008D) Soderberg et al. 2008; (2008ax) Pastorello et al. 2008a.
[b] In all cases, the host galaxy extinction was inferred using a Milky Way extinction law.
[c] The $(V-R)_{10}$ values are estimated from the observed light curves after correcting for the total line-of-sight extinction.
[d] R-band magnitudes estimated from transformation of r-band data using the transformations of Smith et al. (2002).

fits in Figures 2 and 3, respectively, and the estimated epoch and magnitude of maximum light for our sample are listed in Table 5. The Bronze sample do not have sufficient early data to reasonably constrain the epoch and magnitude of the light curve peak through template fitting.

In Figures 7 and 8 we display the absolute magnitude light curves for the P60 Gold and Silver samples after shifting them to the epoch of maximum light and correcting for Galactic extinction ($\langle E(B-V)_{\text{Gal}} \rangle \approx 0.09$ mag for the P60 sample). Similar to the case of the literature sample, we find a broad distribution in $M_{V,\text{peak}}$ and $M_{R,\text{peak}}$ values that span ∼2–3 mag. Dividing the Gold and Silver samples into the SNe Ib, Ic, and Ic-BL (8, 7, and 2 SNe, respectively), we report mean values of $\langle M_{R,\text{peak}} \rangle = -17.4 \pm 0.5$ mag (Ib), $\langle M_{R,\text{peak}} \rangle = -17.5 \pm 0.4$ mag (Ic), and $\langle M_{R,\text{peak}} \rangle = -18.2 \pm 0.5$ mag (Ic-BL). These values are overall consistent with those of the literature sample.

Adopting the fitted parameters for the light curve maxima, we next extract $\Delta m_{15,V}$ and $\Delta m_{15,R}$ values for our Gold and Silver SNe following the same procedure as adopted for the literature sample (Section 3.1). In Table 5, we list the resulting Δm_{15} values for the V and R bands, and in Figure 9 we compare their distributions with those from the literature sample. We find mean values of $\langle \Delta m_{15,V} \rangle = 0.78 \pm 0.11$ mag and $\langle \Delta m_{15,R} \rangle = 0.61 \pm 0.13$ mag, somewhat lower than those derived for the literature sample but consistent within the 1σ uncertainties. Similar to the case of the literature sample, we find no evidence for a statistically significant difference between the decay rates of the SNe sub-classes.

Finally, we comment on the rise time of the SNe Ibc in this sample, i.e., the time interval between the epoch of first detection and the epoch of maximum light. As shown in

Figures 7 and 8, SNe Ibc with broader light curves tend to have correspondingly longer rise times. We find that several SNe in this P60 sample have R-band rise times exceeding 20 days and thus are comparable (even longer) than those observed for SNe Ia (Conley et al. 2006; Hayden et al. 2010). This study emphasizes the dispersion in rise times of SNe Ibc light curves through dense, multi-band photometry of young explosions.

3.3. The Combined Sample

By combining the Gold and Silver P60 samples with the literature sample, we derive mean values for the peak absolute magnitudes and light curve decline rates for a larger sample of SNe Ibc to search for statistical differences. Correcting for Galactic extinction only, we find $M_{V,\text{peak}} = -17.0 \pm 0.9$ mag and $M_{R,\text{peak}} = -17.4 \pm 0.7$ mag. For comparison, Li et al. (2011) recently reported that the typical unfiltered peak absolute magnitudes for SNe Ibc within $d \approx 60$ Mpc are $M_{\text{peak}} = -16.1 \pm 1.1$ mag. Restricting our sample to this same distance, we find a slightly higher value of $M_{R,\text{peak}} = -16.9 \pm 0.6$ mag in the R band, although we note that these values are consistent within the 1σ uncertainties.

Dividing our extended sample into the three spectroscopic sub-classes (12 Ib, 10 Ic, and 5 Ic-BL), we report mean peak magnitudes with higher statistical confidence: $\langle M_{R,\text{peak}} \rangle = -17.0 \pm 0.7$ mag (Ib), $\langle M_{R,\text{peak}} \rangle = -17.4 \pm 0.4$ mag (Ic), and $\langle M_{R,\text{peak}} \rangle = -18.3 \pm 0.6$ mag (Ic-BL). This is in contrast to the report of Li et al. (2011) that SNe Ib are marginally brighter than SNe Ic; we attribute this apparent difference to small number statistics. While the light curve maxima for our sample of Bronze SNe are not well constrained, we are able to place strict lower limits on the peak absolute magnitudes
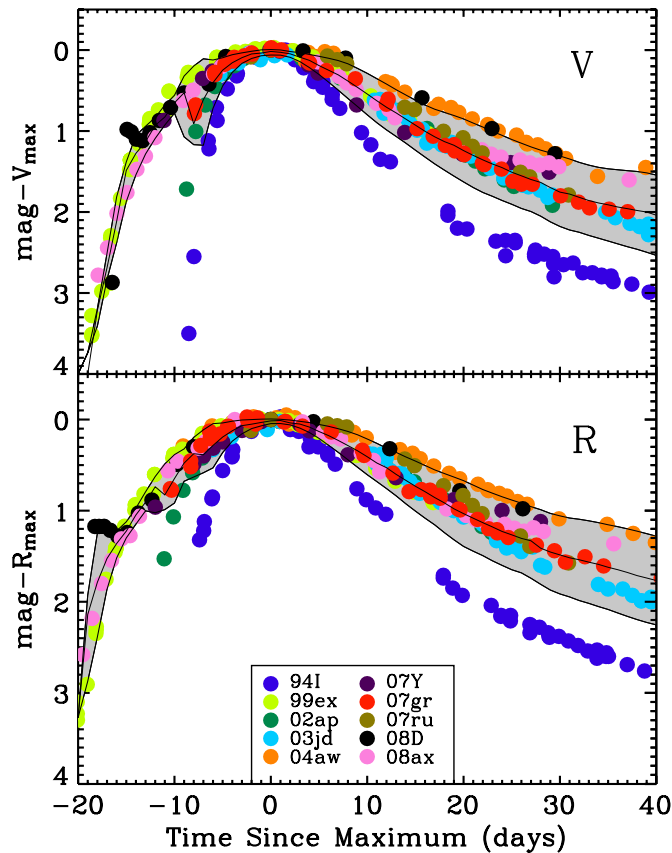
Figure 5. Comparison of the *V*- and *R*-band light curves for the sample of 10 well-studied SNe Ibc currently available in the literature (see Table 3). A compilation of their *V*-band (top panel) and *R*-band (bottom panel) light curves is scaled to their respective epoch of $V_{max}(R_{max})$ and used to construct a mean template light curve (gray curve). The width of the curve is derived from the 1σ deviation from the mean at each epoch.

(A color version of this figure is available in the online journal.)

Figure 6. We extract the Δm_{15} values for the sample of literature SNe in the *V* band (top) and *R* band (bottom). Within each band, we compare the Δm_{15} values for each of the SNe Ib (blue thin lines), Ic (red thin lines), and Ic-BL (red/black dashed lines) assuming Gaussian errors for each of the estimates. We normalize the summed differential distributions to unity producing probability density distributions for SNe Ib, Ic, and Ic-BL (thick lines). A statistical test shows no evidence that the typical Δm_{15} values vary across the sub-classes.

(A color version of this figure is available in the online journal.)

by adopting the brightest data point the *V* and *R* bands and correcting for Galactic extinction. These lower limits range from $M_{V,\text{peak}} = -16.3$ to -18.0 mag and $M_{R,\text{peak}} = -17.1$ to -18.5 mag. In Figure 10, we present the differential distribution of peak absolute magnitudes for our combined sample, including the lower limits derived for the Bronze P60 SNe.

We next calculate mean decay rates for the combined sample of $\langle\Delta m_{15,V}\rangle = 0.87 \pm 0.25$ mag and $\langle\Delta m_{15,R}\rangle = 0.66 \pm 0.20$ mag. Dividing into the sub-classes, we find $\langle\Delta m_{15,R}\rangle = 0.62 \pm 0.14$ mag (Ib), $\langle\Delta m_{15,R}\rangle = 0.73 \pm 0.27$ mag (Ic), and $\langle\Delta m_{15,R}\rangle = 0.60 \pm 0.14$ mag (Ic-BL). A Kolmogorov–Smirnov (K-S) test on these distributions reveals an 89% probability that SNe Ib and Ic are drawn from the same population, and the probability that SNe Ic and Ic-BL are the same is 86%. Summing the SNe Ib and Ic distributions together, a K-S test reveals a 91% probability that SNe Ic-BL are drawn from the ordinary SNe Ibc sample. This study demonstrates that the post-maximum decay rate of SN Ibc optical light curves cannot be used to distinguish between SNe Ib, Ic, and Ic-BL.

4. HOST GALAXY EXTINCTION CORRECTIONS

In Section 3.3, we report the peak absolute magnitudes for our combined sample of SNe Ibc light curves after a typically small correction for Galactic extinction. However, SNe Ibc are known to reside in dusty star-forming regions (van Dyk et al.
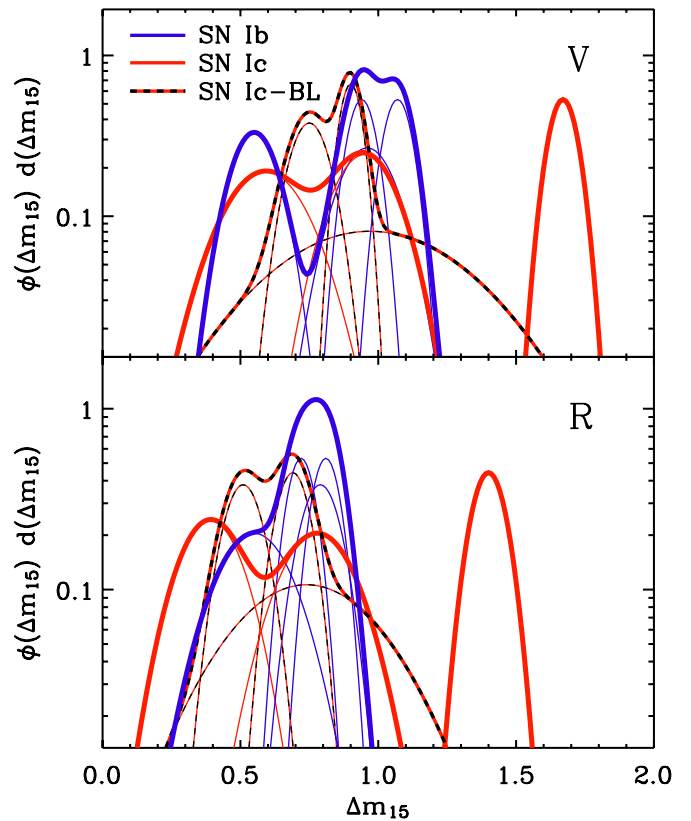
1996; Kelly et al. 2008), and thus extinction within the host galaxy likely dominates the total line-of-sight extinction.

Motivated by the well-studied Lira relation observed for SNe Ia (Phillips et al. 1999), we investigate whether the color evolution of SN Ibc may be used to infer the total line-of-sight extinction. To this end, we construct $(V - R)$ color curves for the literature sample and compare their temporal evolution with respect to the epoch of *V*- and *R*-band light curve maxima. In Figures 11 and 12 (top panels), we display the $(V - R)$ color curves after correcting *only* for Galactic extinction. All of these SNe show a clear trend of increasing $(V - R)$ color beginning $\sim$1 week prior to maximum light; however, there is a broad dispersion in the $(V - R)$ colors at any single epoch.

For each of these literature sample SNe, host galaxy extinction estimates, $E(B - V)_{\text{host}}$, are available based on the equivalent width of the Na I D lines and/or fitting of the spectral energy distribution (Table 4). The respective authors assume an $R_V = 3.1$ Milky Way extinction law for the host galaxy in every case. A comparison of $E(B - V)_{\text{Gal}}$ and $E(B - V)_{\text{host}}$ values for each SN reveals that host galaxy extinction is (nearly) always dominant. Indeed, we find a mean host galaxy extinction of $\langle E(B - V)_{\text{host}}\rangle = 0.21 \pm 0.20$ mag for the literature sample, a factor of $\sim$4 higher than the average Galactic extinction for these same SNe.

By summing the Galactic contribution with the host galaxy extinction estimates, we correct the color curves for the total

Table 5
Light Curve Properties of the P60 Sample

SN	Band	Peak Time (JD)	Peak Apparent Magnitude[a]	Δm_{15} (mag)	$E(B-V)$ Host (mag)	Peak Absolute Magnitude	Group
2004dk	V	2453238.0 ± 0.5	14.76 ± 0.1	0.56 ± 0.12	0.18 ± 0.11	-18.10 ± 0.59	G
	R	2453242.5 ± 0.5	14.42 ± 0.1	0.45 ± 0.13	. . .	-18.18 ± 0.51	. . .
2004dn	V	2453230.5 ± 0.5	17.35 ± 0.1	0.76 ± 0.15	0.52 ± 0.13	-17.95 ± 0.66	G
	R	2453232.0 ± 0.5	16.92 ± 0.1	0.61 ± 0.14	. . .	-17.94 ± 0.56	. . .
2004fe	V	2453318.0 ± 0.5	16.91 ± 0.1	0.87 ± 0.16	0.29 ± 0.11	-18.35 ± 0.59	G
	R	2453320.5 ± 0.5	16.66 ± 0.1	0.80 ± 0.15	. . .	-18.36 ± 0.51	. . .
2004ff	V	. . .	<17.57	. . .	0.27 ± 0.15	< -18.02	S
	R	2453316.0 ± 1.0	17.18 ± 0.2	0.85 ± 0.25	. . .	-18.35 ± 0.60	. . .
2004ge	V	. . .	<17.69	. . .	0.88 ± 0.15	< -19.21	S
	R	2453341.5 ± 1.0	17.09 ± 0.2	0.55 ± 0.27	. . .	-19.31 ± 0.60	. . .
2004gk	V	. . .	<13.98	. . .	>0.030	< -17.20	B
	R	. . .	<13.62	. . .	. . .	< -17.86	. . .
2004gq	V	2453361.0 ± 0.5	15.32 ± 0.1	0.78 ± 0.22	0.18 ± 0.11	-17.55 ± 0.90	G
	R	2453361.5 ± 0.5	14.99 ± 0.1	0.60 ± 0.22	. . .	-17.69 ± 0.82	. . .
2004gt	V	. . .	<15.77	. . .	>0.046	< -16.26	B
	R	. . .	<15.34	. . .	. . .	< -17.34	. . .
2004gv	V	. . .	<18.33	. . .	>0.033	< -16.27	B
	R	. . .	<17.86	. . .	. . .	< -17.17	. . .
2005az	V	. . .	<16.11	. . .	0.43 ± 0.11	< -18.23	S
	R	2453476.0 ± 1.0	15.55 ± 0.2	0.42 ± 0.22	. . .	-18.45 ± 0.56	. . .
2005eo	V	. . .	<17.71	. . .	0.57 ± 0.20	< -18.90	S
	R	2453648.0 ± 1.0	17.25 ± 0.2	0.71 ± 0.25	. . .	-18.87 ± 0.75	. . .
2005hg	V	2453684.0 ± 0.5	17.44 ± 0.1	0.79 ± 0.15	0.58 ± 0.13	-19.36 ± 0.65	G
	R	2453686.0 ± 0.5	16.80 ± 0.1	0.62 ± 0.15	. . .	-19.47 ± 0.55	. . .
2005kz	V	. . .	<18.15	. . .	0.46 ± 0.13	< -18.75	S
	R	2453715.0 ± 1.0	17.61 ± 0.2	0.41 ± 0.29	. . .	-18.89 ± 0.56	. . .
2005la	V	. . .	<18.00	. . .	>0.011	< -16.44	B
	R	. . .	<17.64	. . .	. . .	< -17.10	. . .
2005mf	V	2453736.0 ± 0.5	18.00 ± 0.1	0.78 ± 0.19	0.38 ± 0.12	-18.51 ± 0.62	G
	R	2453737.5 ± 0.5	17.65 ± 0.1	0.66 ± 0.19	. . .	-18.54 ± 0.53	. . .
2005nb	V	. . .	<17.60	. . .	>0.037	< -17.63	B
	R	. . .	<17.05	. . .	. . .	< -18.15	. . .
2006F	V	. . .	<17.70	. . .	0.54 ± 0.17	< -18.27	S
	R	2453754.0 ± 1.0	17.00 ± 0.2	0.74 ± 0.24	. . .	-18.41 ± 0.65	. . .
2006ab	V	. . .	<18.55	. . .	0.27 ± 0.18	< -17.93	S
	R	2453784.5 ± 2.0	17.58 ± 0.2	0.56 ± 0.21	. . .	-18.32 ± 0.67	. . .
2006ck	V	. . .	<18.29	. . .	>0.028	< -17.04	B
	R	. . .	<17.68	. . .	. . .	< -17.91	. . .
2006dn	V	. . .	<17.56	. . .	0.43 ± 0.29	< -18.36	S
	R	2453932.0 ± 1.0	17.07 ± 0.2	0.44 ± 0.26	. . .	-18.43 ± 0.99	. . .
2006el	V	2453982.5 ± 1.0	17.61 ± 0.2	0.73 ± 0.25	0.19 ± 0.12	-17.56 ± 0.79	G
	R	2453984.5 ± 1.0	17.26 ± 0.2	0.57 ± 0.24	. . .	-17.67 ± 0.70	. . .
2006fo	V	. . .	<17.07	. . .	>0.029	< -17.70	B
	R	. . .	<16.65	. . .	. . .	< -18.25	. . .
2006jc	V	. . .	<14.74	. . .	>0.020	< -18.00	B
	R	. . .	<14.70	. . .	. . .	< -18.47	. . .
2007C	V	2454116.5 ± 0.5	16.07 ± 0.1	0.94 ± 0.14	0.64 ± 0.12	-18.04 ± 0.70	G
	R	2454118.0 ± 0.5	15.49 ± 0.1	0.72 ± 0.14	. . .	-18.10 ± 0.61	. . .
2007D	V	. . .	<18.15	. . .	0.91 ± 0.13	< -20.54	S
	R	2454120.0 ± 1.0	17.09 ± 0.2	0.67 ± 0.29	. . .	-20.65 ± 0.55	. . .

Note. [a] Peak apparent magnitude errors are dominated by the uncertainty associated with template fitting for the epoch and magnitude at maximum.

line-of-sight extinction.[15] As shown in Figures 11 and 12 (bottom panels), the dispersion in the resulting $(V - R)$ color curves is significantly decreased after correcting for host galaxy extinction. We construct extinction-corrected template color curves over timescales spanning -20 to $+40$ days since light

curve maxima in both the V and R bands by extracting the mean and standard deviation of the $(V - R)$ color at each epoch. As shown in the figures, the dispersion in the template curves is minimized at roughly $\Delta t \approx 10$ days after the V- and R-band light curve maxima.

Interpolating the color curves to $\Delta t = 10$ days after maximum, we estimate mean values of $\langle (V - R)_{V10} \rangle = 0.26 \pm 0.06$ mag $\langle (V - R)_{R10} \rangle = 0.29 \pm 0.08$ mag and a full range extending from $(V - R)_{V10} \approx 0.18$ to 0.34 mag and

---

[15] We do not include a k−correction to the $E(B - V)_{\text{host}}$ values since (1) the SNe all reside in the local universe, and (2) the uncertainties in the host galaxy extinction values are often significant.
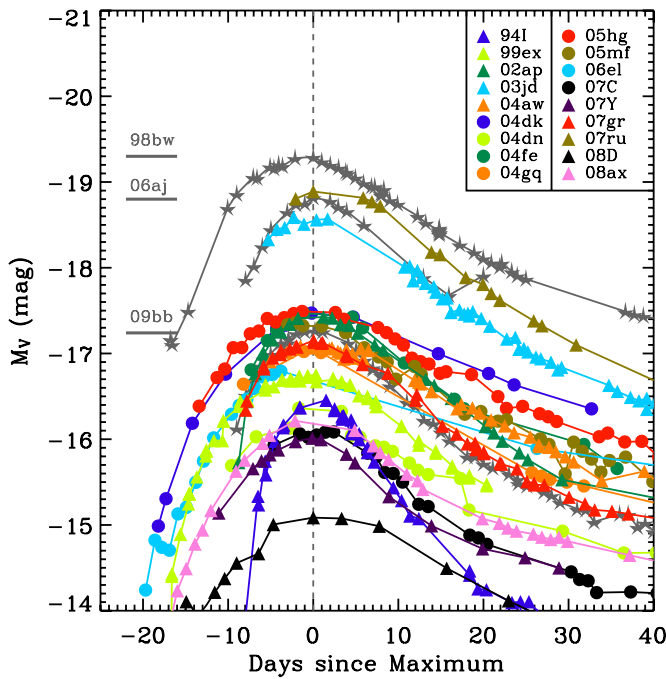
Figure 7. Absolute *V*-band light curves for our Gold SNe Ibc and literature sample, *before* correcting for host galaxy extinction. The light curves for engine-driven SNe 1998bw, 2006aj, and 2009bb are indicated by gray star symbols and the peak magnitudes are labeled by gray bars.

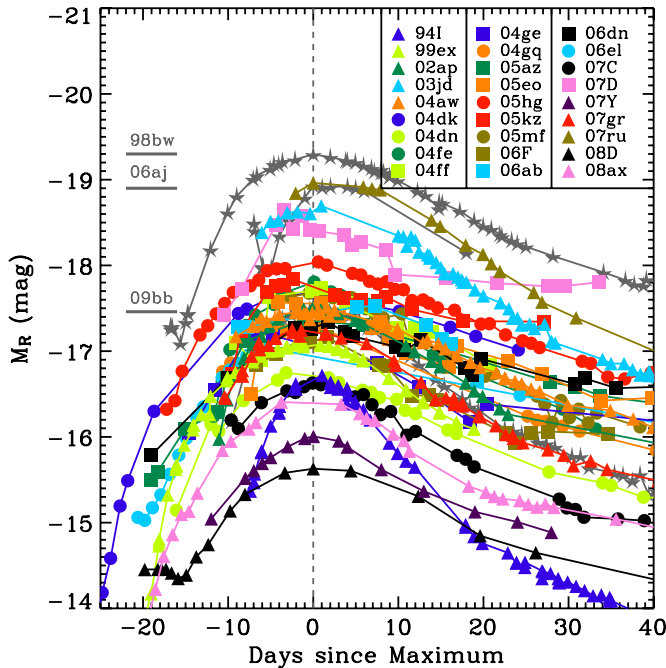(A color version of this figure is available in the online journal.)

Figure 8. Absolute *R*-band light curves for our Gold and Silver SNe Ibc and literature sample, *before* correcting for host galaxy extinction. The light curves for engine-driven SNe 1998bw, 2006aj, and 2009bb are indicated by gray star symbols and the peak magnitudes are labeled by gray bars.

(A color version of this figure is available in the online journal.)

$(V - R)_{R10} \approx 0.20$ to 0.44 mag. We conclude that the $(V - R)$ color evolution observed for SNe Ibc can be exploited as a useful diagnostic for estimating their host galaxy extinction.

We adopted these extinction-corrected mean colors and their associated dispersions at $\Delta t \approx 10$ days as template values and
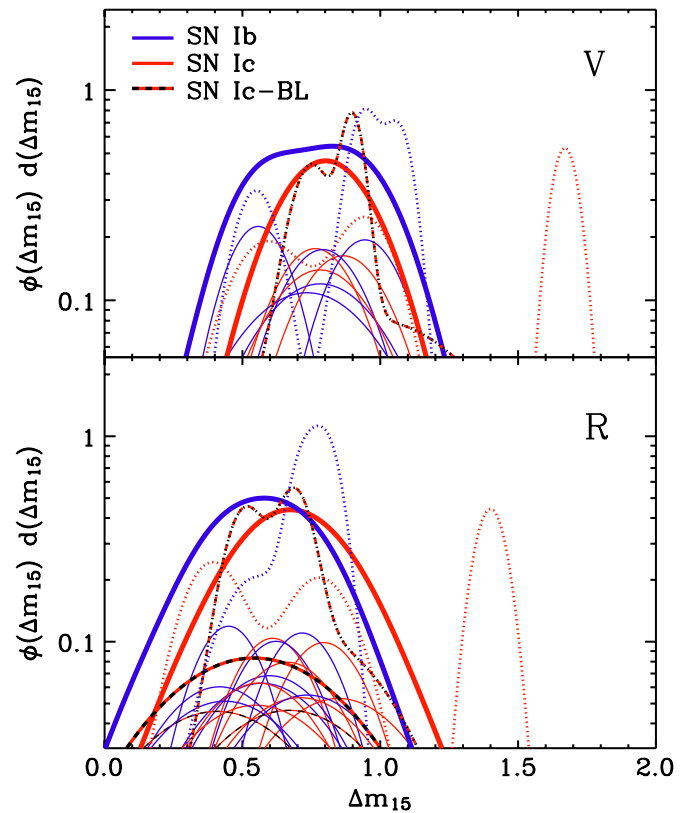
Figure 9. We extracted the Δm_{15} values for our Gold SNe in the *V* and *R* bands and in the *R* band for the Silver SNe. In each band, we compare the Δm_{15} estimates for SNe Ib (thin blue lines), Ic (thin red lines), and Ic-BL (red/black dashed lines) assuming Gaussian errors. We normalize the summed differential distributions to unity (thick lines). For comparison, we overplot the summed differential distributions from the literature sample (Figure 6; dotted lines). The Δm_{15} distributions are similar for the literature and P60 samples, across the sub-classes.

(A color version of this figure is available in the online journal.)

used them to infer the total host galaxy extinction for our P60 sample. To this end, we first constructed $(V - R)$ color curves for the P60 sample and corrected each for Galactic extinction (see Table 1). We interpolated over the P60 color curves to estimate the respective values of $(V - R)_{V10}$ and $(V - R)_{R10}$ for all Gold SNe and $(V - R)_{R10}$ for all Silver SNe. By attributing any residual color excess over the template values to host galaxy extinction, we derived $E(B - V)_{\mathrm{host}}$ estimates for each SN.

As shown in Figures 13–15, the extinction-corrected color curves for our P60 sample are generally consistent with the template curves constructed from the literature sample. The host galaxy extinction values are listed in Table 5, where the associated uncertainties are dominated by the standard deviation of the template values at 10 days after *V*- and *R*-band maxima. To ensure consistency with the literature sample extinction estimates, we similarly adopted a Milky Way extinction law for the host galaxies.

We combine the $E(B - V)_{\mathrm{host}}$ values for the literature and P60 samples and report a mean extinction of $E(B - V)_{\mathrm{host}} = 0.36 \pm 0.24$ mag. Dividing the sample into spectroscopic sub-classes, we find no evidence for a statistically significant difference in their host galaxy extinction values. A K-S test reveals that the probability that SNe Ib, Ic, and Ic-BL are drawn from the same population of events is $\gtrsim 17\%$. Therefore, based on our compilation of *V*- and *R*-band light curves from the literature and our P60 study, we conclude that most SNe
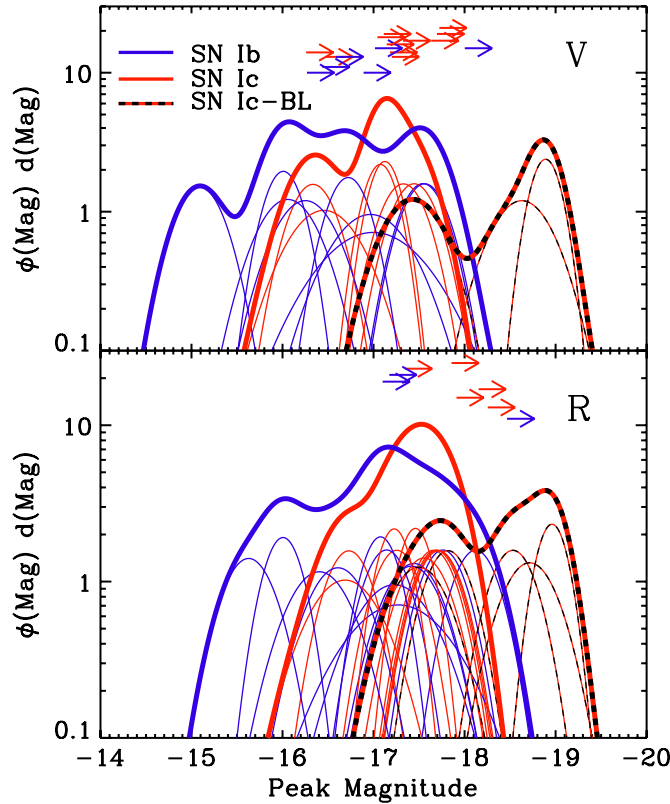
Figure 10. Comparison of the peak absolute magnitudes in the *V* and *R* bands for SNe Ib (blue thin lines), Ic (red thin lines), and Ic-BL (red/black dashed lines) from the Gold and Silver P60 and literature samples *before* correcting for host galaxy extinction. We assume that the errors are Gaussian and that the area under each thin curve is normalized to one. The thick lines are the summed differential distributions for SNe Ib, Ic, and SNe Ic-BL (thick lines). Lower limits on the peak absolute magnitudes are shown by arrows for the Bronze P60 sample.

(A color version of this figure is available in the online journal.)

Ibc show evidence for significant host galaxy extinction. This is slightly higher than the extinction estimates for SNe IIP ($\langle A_V \rangle \approx 0.9$ mag; Smartt et al. 2009), suggesting that SNe Ibc tend to be more embedded in the star-forming regions of their host galaxies than SNe IIP and consistent with the results of Kelly et al. (2008). Finally, we note that this result is broadly consistent with the extinction estimates derived systematically from optical and near-IR afterglow studies of a sample of long-duration GRBs (Perley et al. 2009; Greiner et al. 2010).

4.1. Consistency with Independent Extinction Estimates

For the SNe from our sample with high $E(B-V)_{host}$ estimates, we searched for an indication of high equivalent width Na I D absorption features which have been shown to correlate with total line-of-sight extinction (e.g., Munari & Zwitter 1997). Indeed, in the case of our highest extinction SNe, ($E(B-V) \gtrsim 0.9$ mag), strong Na I D features ($EQ \gtrsim 0.1$ nm) at the redshift of the host galaxies were detected in the initial classification spectra: SNe 2004ge (Filippenko & Foley 2004) and 2007D (R. J. Foley & Gal-Yam 2010, private communication).[16] These independent extinction diagnostics support our photometry-based technique.

---

[16] We caution, however, that the uncertainty in the extinction correction likely increases for the more highly extinguished SNe (e.g., Blondin et al. 2009).
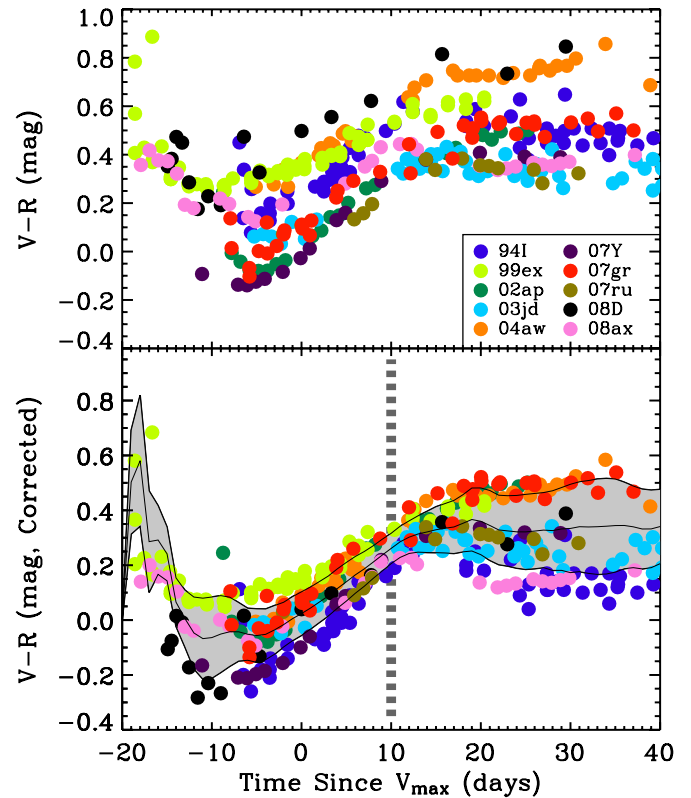

Figure 11. We compare the $(V-R)$ color evolution in days since *V*-band maximum light for the sample of 10 well-studied SNe Ibc currently available in the literature (see Table 3). Top: $(V-R)$ color evolution after correcting for Galactic extinction only. Bottom: $(V-R)$ color evolution after correcting for Galactic and host galaxy extinction. The dispersion in the color evolution is decreased by accounting for the (often large) host galaxy extinction with a minimum dispersion observed on a timescale of roughly 10 days after the observed epoch of $M_{V,peak}$ (dashed gray line) with mean value of 0.26 ± 0.06 mag (gray curve).

(A color version of this figure is available in the online journal.)

4.2. Host Galaxy Inclination

To investigate the proximity of the dust to the explosion site, we compare the host galaxy inclination and the $E(B-V)_{host}$ values. We estimate the inclination for each host galaxy in the literature and P60 samples using the traditional formalism of Hubble (1926), adopting the major and minor host galaxy axes from de Vaucouleurs et al. (1991). In Figure 16, we compare the host inclinations with the derived $E(B-V)_{host}$ values. A general trend is seen whereby the more heavily extinguished SNe reside within more highly inclined host galaxies. A similar result was recently reported by Li et al. (2011) based on the distribution of peak absolute magnitudes prior to host galaxy extinction corrections. We find evidence for a significant correlation (94% confidence level) between host inclination and extinction with a Spearman correlation coefficient of $\rho \approx 0.37$. As the figure reveals, however, there is (at least) one notable exception to this trend, the highly extinguished Type Ic SN 2004ge and its nearly face-on galaxy, UGC 3555. There is also evidence that some SNe (e.g., Type Ibn) form significant dust through the dynamical interaction of the SN blastwave with the local environment (Smith et al. 2008). We conclude that dust within the host galaxy dominates the derived $E(B-V)_{host}$ values for SNe Ibc, but local dust ($\lesssim 1$ kpc) may contribute significantly in some cases.
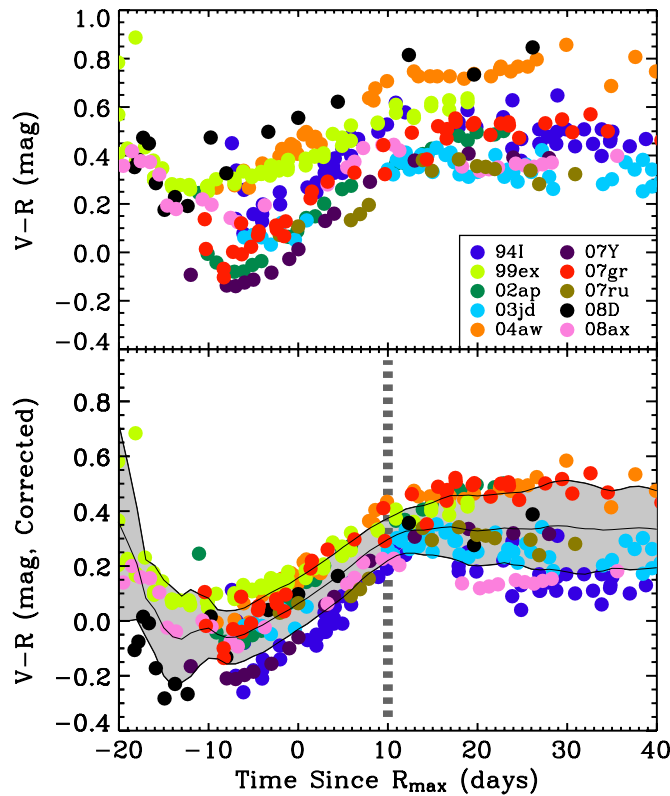
Figure 12. We compare the $(V - R)$ color evolution in days since R-band maximum light for the sample of 10 well-studied SNe Ibc currently available in the literature (see Table 3). Top: $(V - R)$ color evolution after correcting for Galactic extinction only. Bottom: $(V - R)$ color evolution after correcting for Galactic and host galaxy extinction. The dispersion in the color evolution is decreased by accounting for the (often large) host galaxy extinction with a minimum dispersion observed on a timescale of roughly 10 days after the observed epoch of $M_{R,\mathrm{peak}}$ (dashed gray line) with mean value of 0.29 ± 0.08 mag (gray curve).

(A color version of this figure is available in the online journal.)

Figure 13. We compare the $(V - R)$ color evolution in days since V-band maximum light for our sample of Gold SNe Ibc after correcting for Galactic extinction only (top) and the total extinction (bottom) as estimated using the intrinsic $(V - R)_{V10}$ colors for well-studied SNe Ibc from the literature (gray band).

(A color version of this figure is available in the online journal.)

5. EXTINCTION CORRECTED PEAK LUMINOSITIES

We next construct a sample of *total* extinction-corrected light curves by correcting for the $E(B - V)_{\mathrm{host}}$ values compiled in Tables 4 and 5. The corrected V- and R-band light curves are shown collectively in Figures 17 and 18. From this combined sample, we derive the mean, total extinction-corrected peak R-band magnitude of all SNe Ibc to be $\langle M_{R,\mathrm{peak}} \rangle = -18.2 \pm 0.9$ mag. Focusing on the SNe Ibc within $d \approx 60$ Mpc, we find a value of $\langle M_{R,\mathrm{peak}} \rangle = -17.6 \pm 0.6$ mag. A direct comparison with the values discussed in Section 3.3 reveals the importance of including host galaxy extinction corrections in deriving the luminosity function for SNe Ibc (cf. Li et al. 2011).

The differential distribution of corrected peak absolute magnitudes for the combined sample is shown in Figure 19. We note that the errors on these estimates are fairly large (e.g., ± 0.5 mag) since we have properly accounted for the uncertainties in host galaxy distance, host galaxy extinction correction, and photometric measurement error. Dividing the sample into SNe Ib and ordinary SNe Ic, we find $\langle M_{R,\mathrm{peak}} \rangle = -17.9 \pm 0.9$ mag (Ib) and -18.5 ± 0.8 mag (Ic).

As shown in Figure 20, the cumulative distributions of total extinction-corrected R_{max} values for SNe Ib and Ic indicate that they are similar; a K-S test reveals a 36% probability that these events are from the same parent population of explosions. Thus, we find no statistical evidence for a difference in the peak
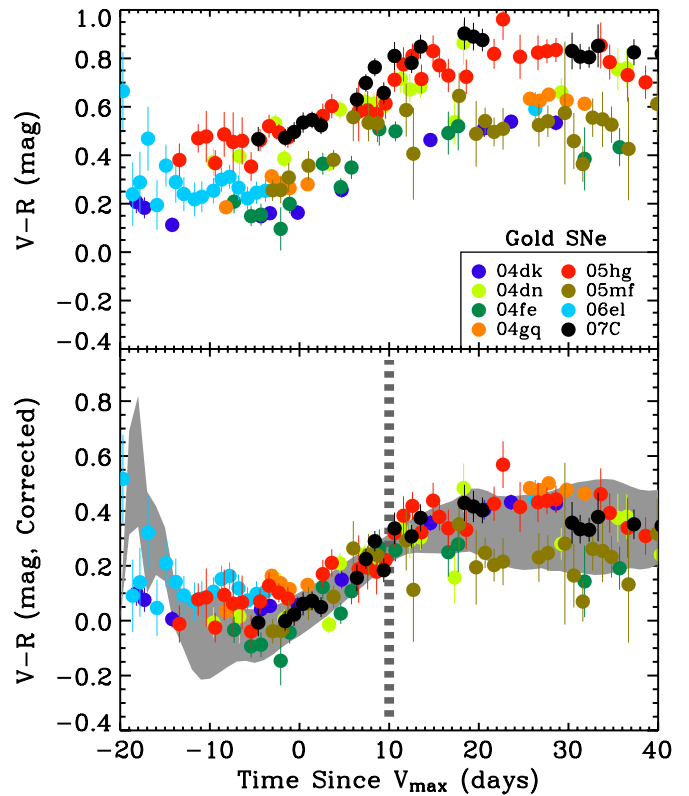
luminosities of He-rich and He-poor explosions. As discussed in Section 6, this suggests that SNe Ib and Ic synthesize a similar mass of ^{56}Ni.

Separating out the broad-lined SNe Ic, we next compare their peak luminosities with ordinary SNe Ic and Ib. While the sample is small, a K-S test reveals only a 1.6% probability that they are drawn from the same population of explosions. We report a mean, total extinction-corrected, peak absolute magnitude for SNe Ic-BL of $\langle M_{R,\mathrm{peak}} \rangle = -19.0 \pm 1.1$ mag, comparable to those of SNe Ia (Riess et al. 1999). We further note that none of these SNe show evidence for a central engine, which may be revealed through the detection of an associated GRB and/or strong non-thermal synchrotron emission (an afterglow) from a relativistic blastwave (see Soderberg et al. 2006b and references therein).

Our peak magnitudes are roughly consistent with the broad range of values reported by Richardson et al. (2006) based on their compilation of SN Ibc light curves available in the literature. However, we do not confirm evidence for a bimodal distribution of peak absolute magnitudes and suggest that this may be due to a disproportionate representation of overluminous SNe in their literature compilation.

Finally, in Figure 21, we compare the peak absolute magnitudes in the V and R bands with their associated $\Delta m_{15,V}$ and $\Delta m_{15,R}$ estimates. In contrast to SNe Ia where Δm_{15} is seen to correlate tightly with $M_{V,\mathrm{peak}}$, we find no evidence for a "Phillips relation" in our sample of SNe Ibc. We calculate a Spearman correlation coefficient of $\rho \approx 0.058$ with a confidence level of 23%. We therefore conclude that the decline rate of SNe Ibc
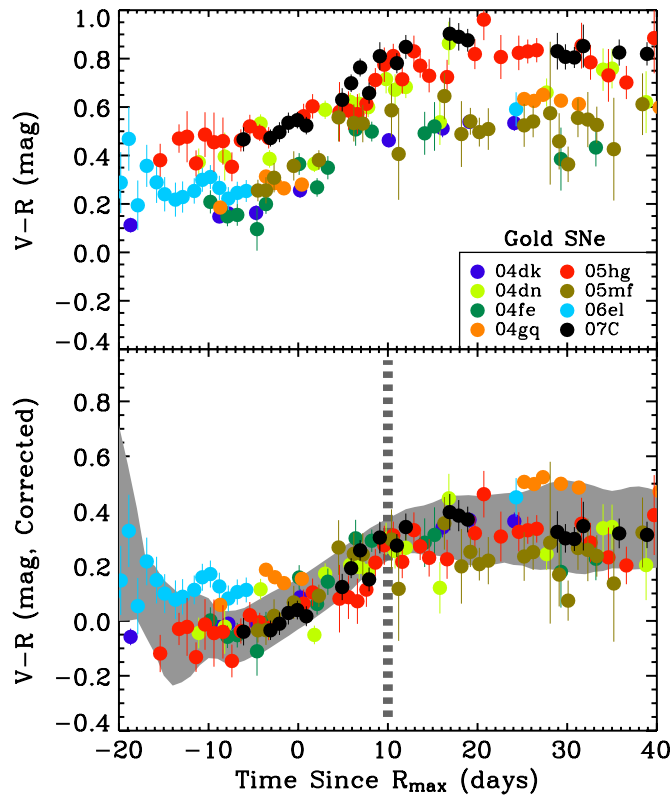
Figure 14. We compare the $(V − R)$ color evolution in days since R-band maximum light for our sample of Gold SNe Ibc after correcting for Galactic extinction only (top) and the total extinction (bottom) as estimated using the intrinsic $(V − R)_{R10}$ colors for well-studied SNe Ibc from the literature (gray band).

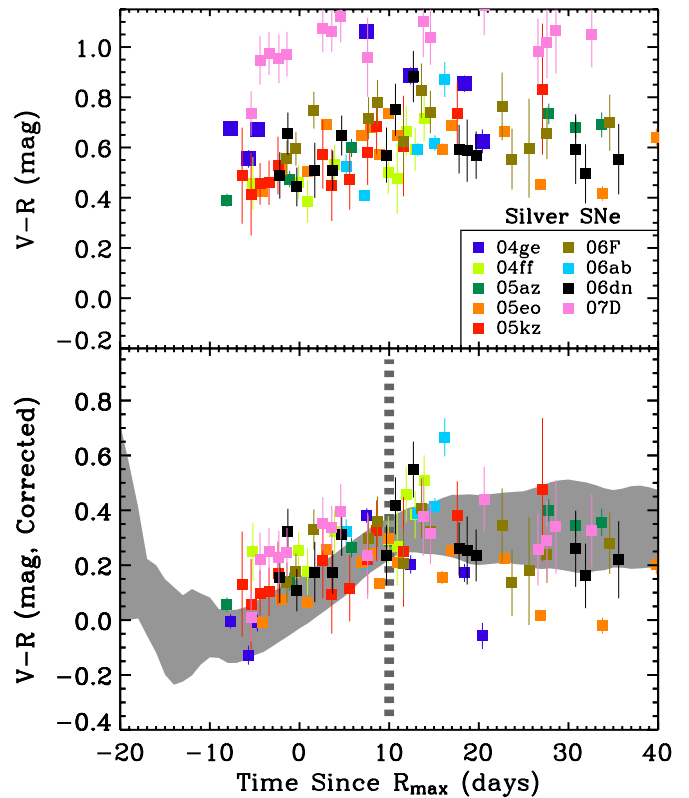(A color version of this figure is available in the online journal.)

Figure 15. We compare the $(V − R)$ color evolution in days since R-band maximum light for our sample of Silver SNe Ibc after correcting for Galactic extinction only (top) and the total extinction (bottom) as estimated using the intrinsic $(V − R)_{R10}$ colors for well-studied SNe Ibc from the literature (gray band).

(A color version of this figure is available in the online journal.)

light curves cannot be used as a reliable proxy for the peak absolute magnitude and discuss this point further in the context of analytical models in Section 6.

5.1. The Bronze Sample

We note that none of the SNe in our sample show unusual light curve shapes with the exception of two Bronze SNe, 2005la and 2006jc, whose unusual photometric and spectroscopic properties have already been discussed in detail in the literature (Foley et al. 2007; Pastorello et al. 2007, 2008b). We consider the various effects plaguing the Bronze sample and leading to their poor light curve coverage. The Bronze SNe, on average, are *not* characterized by larger distances, higher $E(B − V)_{Gal}$ values, or higher host galaxy inclinations than the other SNe in our sample. We also note that the Bronze group is not populated by intrinsically faint SNe since the lower limits on the peak absolute magnitudes imply $M_{R,peak} \lesssim -17$ mag (Figure 19). We conclude that the lack of early-time data for the Bronze sample is related to the insufficient cadence of many SN discovery surveys, which determines the epoch of first detection.

5.2. A Comparison to Engine-driven SNe

We next compared the optical luminosities of our SN Ibc sample to those of GRB-SNe discovered within a similar volume, $d \lesssim 150$ Mpc. While additional GRB-SNe are available in the literature we chose a distance-limited approach in an effort to minimize observational biases associated with the γ-ray discovery of GRB-SNe. Our comparison GRB-SNe sample
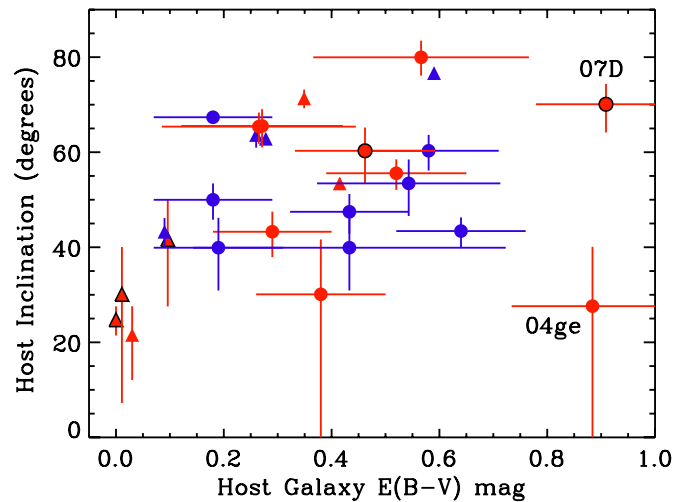
Figure 16. Inferred total line-of-sight extinctions, $E(B − V)$, for SNe Ib (blue), Ic (red), and Ic-BL (red encircled black) are compared with their host galaxy inclinations. A general trend is seen with the more heavily extinguished SNe residing in more highly inclined host galaxies with a 94% confidence level. The two SNe with the highest inferred extinctions, SNe 2004ge and 2007D (labeled), show evidence for unusually strong Na I D lines in their optical spectra, thus supporting our photometrically derived extinction estimates.

(A color version of this figure is available in the online journal.)

includes only two events: SN 1998bw (Galama et al. 1998) associated with GRB 980425 (Pian et al. 2000) at $d \approx 38$ Mpc and SN 2006aj (Pian et al. 2006) associated with XRF 060218 at $d \approx 141$ Mpc. To this small sample of central engine-
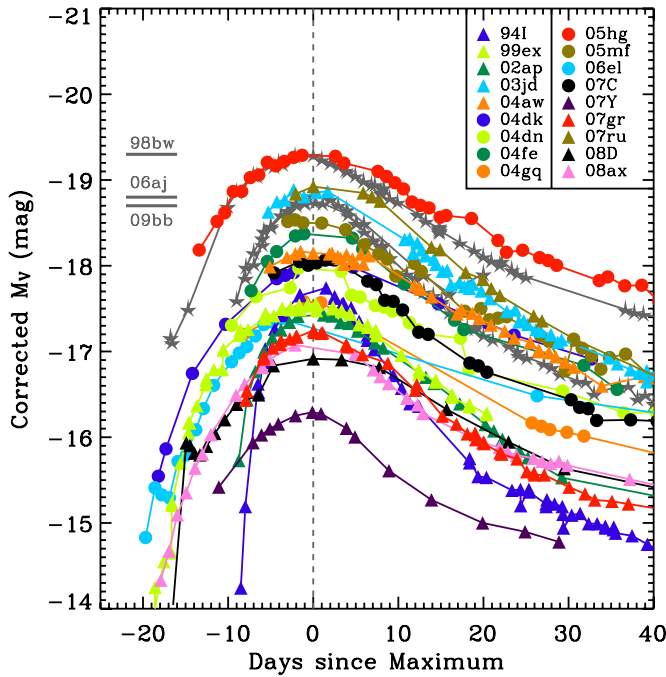
Figure 17. Absolute *V*-band light curves for our Gold SNe Ibc and literature sample, *after* correcting for host galaxy extinction. The symbols are the same as those in Figure 7. The extinction-corrected light curves for engine-driven SNe 1998bw, 2006aj, and 2009bb are indicated by gray star symbols and the peak magnitudes are labeled by gray bars.

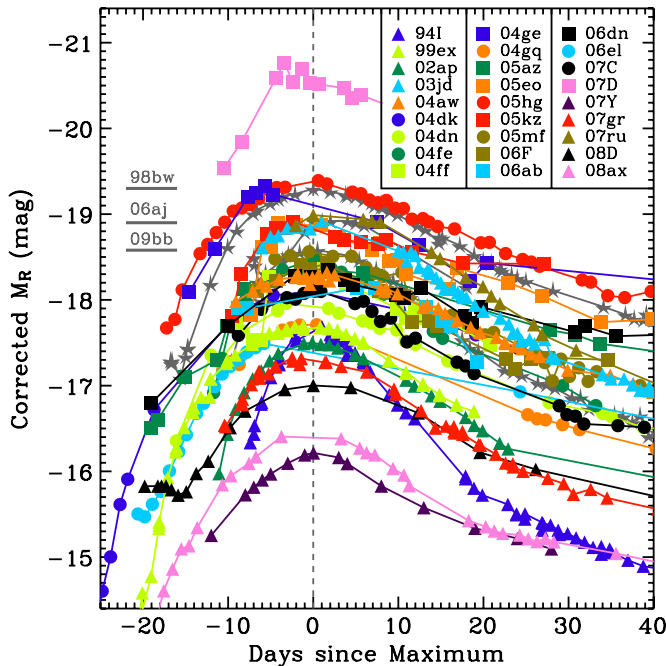(A color version of this figure is available in the online journal.)

Figure 18. Absolute *R*-band light curves for our Gold and Silver SNe Ibc and literature sample, *after* correcting for host galaxy extinction. The symbols are the same as those in Figure 8. The extinction-corrected light curves for engine-driven SNe 1998bw, 2006aj, and 2009bb are indicated by gray star symbols and the peak magnitudes are labeled by gray bars.

(A color version of this figure is available in the online journal.)

drive explosions, we add the broad-lined Type Ic SN 2009bb at $d \approx 40$ Mpc which was not associated with a detected gamma-ray burst but was shown to produce copious relativistic ejecta based on radio observations of the "orphaned" afterglow (Soderberg et al. 2010).
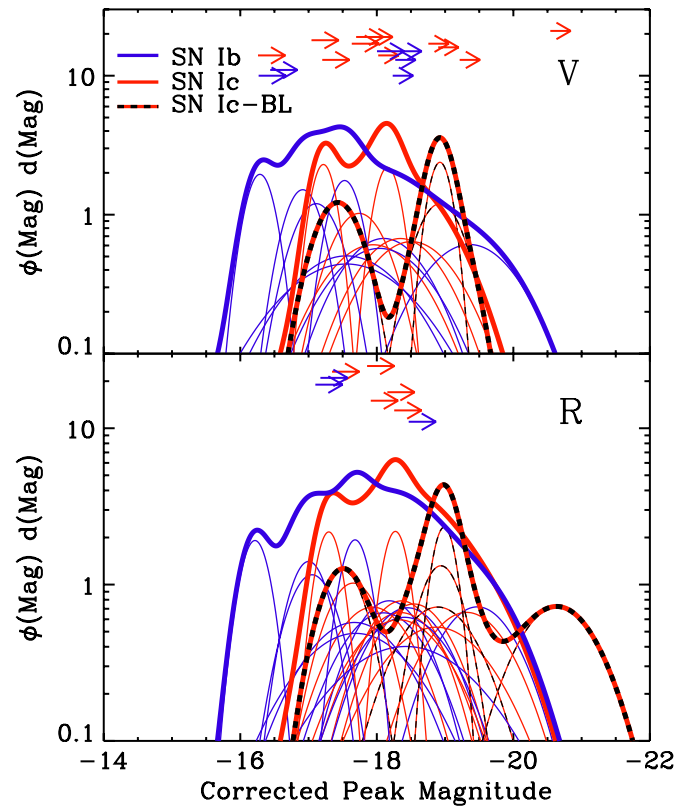

Figure 19. Comparison of the peak absolute magnitudes in the *V* and *R* bands for SNe Ib (blue thin lines), Ic (red thin lines), and Ic-BL (red/black dashed lines) from the Gold and Silver P60 and literature samples *after* correcting for host galaxy extinction. We assume that the errors are Gaussian and that the area under each thin curve is normalized to one. The thick lines are the summed differential distributions for SNe Ib, Ic, and SNe Ic-BL (thick lines). Lower limits on the peak absolute magnitudes are shown by arrows for the Bronze P60 sample and do not include a correction for host galaxy extinction.

(A color version of this figure is available in the online journal.)

We compiled the optical SN photometry in the *V* and *R* bands for SNe 1998bw, 2006aj, and 2009bb from Galama et al. (1998), Mirabal et al. (2006), and Pignata et al. (2011), respectively. After correcting for Galactic extinction, the peak magnitudes for GRB-SNe 1998bw (2006aj) are $M_{V,\text{peak}} \approx -19.3$ (-18.8) mag and $M_{R,\text{peak}} \approx -19.3$ (-18.9) mag. No evidence for host galaxy extinction was reported for either SN 1998bw or SN 2006aj and we test this result using our $(V - R)$ color diagnostic. Interpolating over the light curves, we find $(V - R)_{V10} = 0.25 \pm 0.09$ and 0.34 ± 0.08 mag for SNe 1998bw and 2006aj, respectively. Indeed, these values are consistent with the *total* extinction corrected colors for our literature sample. This exercise serves as independent confirmation for negligible host galaxy extinction in these two cases. The peak magnitudes for SN 2009bb are nearly identical to those of SN 2006aj after correcting for a host galaxy extinction of $E(B - V)_{\text{host}} \approx 0.48$ mag (Pignata et al. 2011). Finally, we note that the recent photometric study of SN 2010bh associated with XRF 100316D further supports the utility of our $(V - R)_{10}$ extinction correction technique for engine-driven SNe with moderate reddening (Cano et al. 2011).

A comparison of the extinction-corrected peak absolute magnitudes for engine-driven SNe and ordinary SNe reveals a handful of objects with luminosities comparable to and/or higher than SNe 1998bw, 2006aj, and 2009bb. We use a Monte Carlo test to determine whether the peak absolute luminosities of these three engine-driven and relativistic SNe are consistent
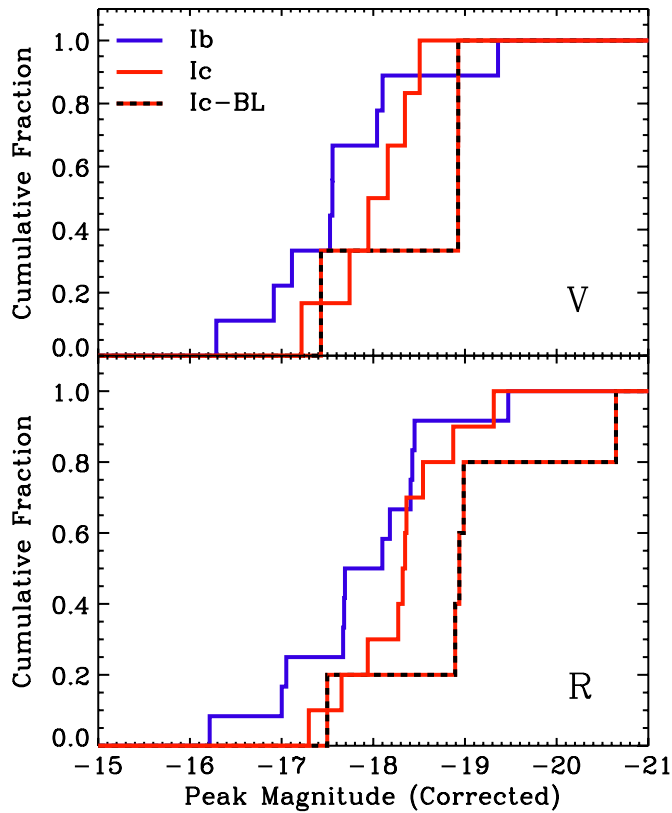
Figure 20. Comparison of the cumulative distributions of peak absolute magnitude in the *V* and *R* bands for SNe Ib (blue), Ic (red), and Ic-BL (red/black) *after* correcting for Galactic and host galaxy extinction. A K-S test reveals a 36% probability that SNe Ib and Ic are drawn from the same population of explosions while the probability that the SN Ic-BL distribution is consistent with ordinary SNe Ibc is just 1.6%.

(A color version of this figure is available in the online journal.)

Figure 21. Comparison of the peak absolute magnitudes in the *V* (top) and *R* bands (bottom) for SNe Ib (blue) and Ic (red) with their respective Δm_{15} values. SNe Ic-BL are emphasized with outlined symbols and engine-driven SNe are indicated by red stars. There is no evidence for a statistically significant correlation between the observed parameters as is seen for SNe Ia.

(A color version of this figure is available in the online journal.)

with the $M_{R,\mathrm{peak}}$ distribution for SNe Ibc (Figure 19). We find a $\sim$2.3% probability that the engine-driven SNe are drawn from the ordinary SNe Ibc population and a $\sim$22% chance that they are consistent with the SNe Ic-BL sample.

6. PHYSICAL PARAMETERS

In this paper, we derived the light curve properties (peak luminosity and decay rate) in a systematic fashion for the 17 Gold and Silver P60 SNe, the 10 well-studied SNe Ibc currently available from the literature, and the three central engine-driven SNe identified to date within the same volume. As discussed in Section 3, these observed properties are directly determined by the three explosion parameters: M_{Ni}, M_{ej}, and E_K. Here we present a systematic method to map the observed light curve properties of SNe Ibc (M_R, Δm_{15}) to the physical parameters of the explosion.

We adopt the analytic light curve models of Valenti et al. (2008), which are based on original formalism of Arnett (1982) for Type I SNe. The models account for the energy deposition of ^{56}Co in addition to ^{56}Ni. We assume a homogeneous density distribution within the SN ejecta and a fixed optical opacity ($\kappa = 0.05\,\mathrm{g\,cm^{-2}}$) to produce a family of 1000 model light curves for a wide range of reasonable explosion parameters spanning $E_K \approx (0.5\text{--}50) \times 10^{51}$ erg, $M_{\mathrm{ej}} \approx 0.1\text{--}10\,M_{\odot}$, and $M_{\mathrm{Ni}} = 0.05\text{--}1.5\,M_{\odot}$. We made the further requirement that $M_{\mathrm{Ni}} \lesssim 0.5 M_{\mathrm{ej}}$ and converted the resulting bolometric light curves to the R band assuming a typical near-IR contribution of $\sim$25% at maximum light (e.g., Stritzinger et al. 2009).
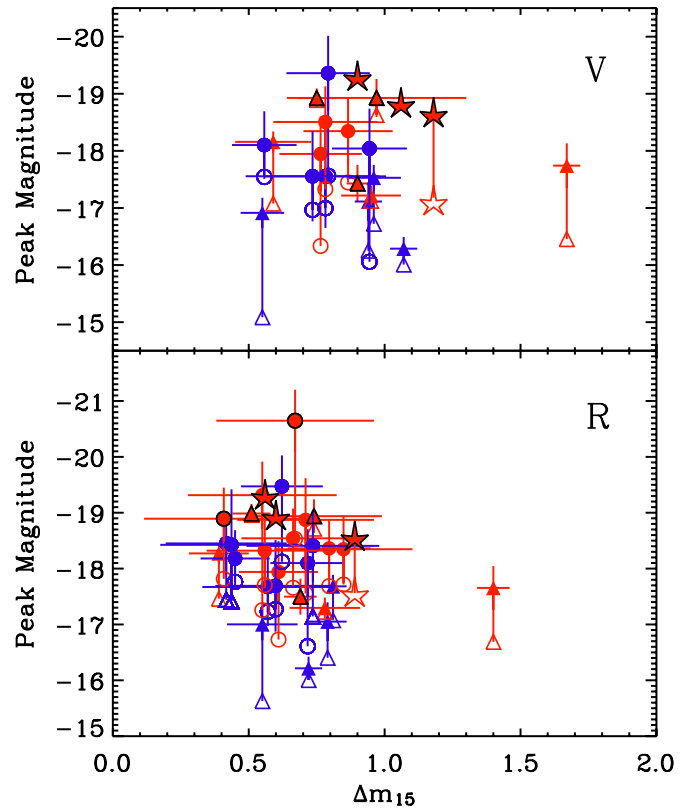
For each model light curve (associated with specific values of M_{Ni}, M_{ej}, and E_K), we *measure* the $\Delta m_{15,R}$ and $M_{R,\mathrm{peak}}$ values. These two measurable quantities define a two-dimension region in the M_{Ni} and τ_c parameter space since a normalization constant is all that distinguishes τ_c from the quantity, $M_{\mathrm{ej},\odot}^{3/4} E_{K,51}^{-1/4}$. Therefore, within this parameter space, the two observable light curve properties are mapped to the three physical explosion parameters (Figure 22). A photospheric velocity measurement is additionally required to break the degeneracy between M_{ej} and E_K.

In Figure 22, we compare the $\Delta m_{15,R}$ and $M_{R,\mathrm{peak}}$ measurements for our sample of SNe Ibc with the grid of synthetic values measured for our family of model light curves. The utility of this figure is that it enables the explosion parameters to be reasonably and systematically estimated using only the two observed quantities and sparing detailed modeling of the light curves and spectra. Extrapolating over the grid of synthetic parameters ($M_{R,\mathrm{peak}}$, $\Delta m_{15,R}$) for the family of models, we convert our measurements to estimates for M_{Ni}, τ_c, and $M_{\mathrm{ej},\odot}^{3/4} E_{K,51}^{-1/4}$ for the SNe in our Gold and Silver P60 samples (Table 6). For a few of the literature SNe and engine-driven SNe, detailed modeling of the light curves and spectra have resulted in direct estimates for the M_{Ni}, M_{ej}, and E_K values (e.g., 1994I; Nomoto et al. 2001, 2002ap; Mazzali et al. 2007a, 1998bw; Iwamoto et al. 1998, 2006aj; Mazzali et al. 2006, and 2008D; Soderberg et al. 2008). In these cases, our inferred physical parameter estimates from Figure 22 are reasonably consistent with the values derived from detailed modeling, thereby supporting our method.
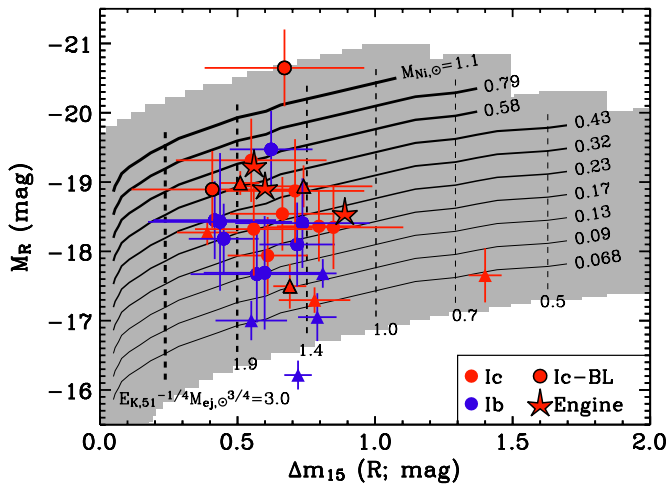
Figure 22. Production of a two-dimensional parameter space for M_R and $\Delta m_{15,R}$ based on a range of reasonable values for M_{Ni}, M_{ej}, and E_K (gray region; see Section 6). The M_{Ni} values are shown by increasing thickness from bottom to top (solid lines). The quantity $E_{K,51}^{-1/4} M_{ej,\odot}^{3/4}$ scales with τ_c and $\Delta m_{15,R}$ and shown in decreasing thickness from left to right (dashed lines). The utility of this figure is that it enables the explosion parameters to be reasonably and systematically estimated without detailed modeling of the light curves and spectra.

(A color version of this figure is available in the online journal.)

6.1. Nickel Masses

We report mean ^{56}Ni masses for SNe Ib of $\langle M_{Ni} \rangle = 0.20 \pm 0.16\ M_\odot$ and for SNe Ic of $\langle M_{Ni} \rangle = 0.24 \pm 0.15\ M_\odot$, while for SNe Ic-BL we find $\langle M_{Ni} \rangle = 0.58 \pm 0.55\ M_\odot$. For comparison, we note that the typical ^{56}Ni masses measured for SNe Ia and IIP are $M_{Ni} \approx 0.5\ M_\odot$ (Mazzali et al. 2007b) and $M_{Ni} \approx 0.07\ M_\odot$, respectively (Nomoto et al. 2006).

A K-S test on the M_{Ni} estimates reveals a 31% probability that SNe Ib and ordinary Ic are drawn from the same group of explosions. Meanwhile, a K-S test on SNe Ic-BL and ordinary SNe Ic reveals only a 3.9% probability of originating from the same population. After grouping SNe Ib and ordinary Ic together, their difference from SNe Ic-BL is accentuated; a K-S test shows only a 1.6% probability that they represent the same explosions.

Focusing on the nearby engine-driven SNe, we find an average ^{56}Ni mass of $M_{Ni} = 0.40 \pm 0.18\ M_\odot$ for the three local events. Based on these M_{Ni} values, we calculate a 10% probability that engine-driven SNe are drawn from the overall SNe Ibc population and a 40% probability that they are drawn from the SNe Ic-BL population. We conclude that SNe Ib and Ic are characterized by similar ^{56}Ni mass values while SNe Ic-BL appear more extreme, bearing more similarity to engine-driven explosions. In this context, we note that the especially bright Type Ic-BL SN 2007D synthesized an estimated ^{56}Ni mass of $M_{Ni} \approx 1.5\ M_\odot$, and the peak luminosity is comparable to the pair-instability candidate, SN 2007bi (Gal-Yam et al. 2009).

In Figure 23, we compare the derived estimates for M_{Ni} with their observed $M_{R,peak}$ values. A clear trend is seen with an intrinsic scatter due to the observed dispersion in light curve width. The relation can be fit by the function, $\log(M_{Ni,\odot}) \approx -0.41\ M_{R,peak} - 8.3$. This function has roughly the same slope as the fit to a literature sample of core-collapse SNe by Perets et al. (2010) but it is somewhat brighter. For future studies of SNe Ibc in which only an extinction-corrected $M_{R,peak}$ value is known, this relation can be used to estimate M_{Ni} in a systematic way.

Table 6
Physical Parameters of the SN Ejecta

SN	τ_c (days)	$M_{ej,\odot}^{3/4} E_{K,51}^{-1/4}$ $(M_\odot)^{3/4}(10^{51}\,\mathrm{erg})^{-1/4}$	M_{Ni} $(M_\odot)$
1994I	$4.8^{+0.3}_{-0.3}$	$0.60^{+0.04}_{-0.04}$	$0.06^{+0.03}_{-0.03}$
1999ex	10^{+1}_{-1}	$1.3^{+0.1}_{-0.1}$	$0.1^{+0.02}_{-0.02}$
2002ap	12^{+1}_{-1}	$1.5^{+0.1}_{-0.1}$	$0.09^{+0.03}_{-0.03}$
2003jd	11^{+5}_{-3}	$1.4^{+0.6}_{-0.4}$	$0.34^{+0.11}_{-0.08}$
2004aw	19^{+4}_{-3}	$2.3^{+0.5}_{-0.4}$	$0.27^{+0.05}_{-0.05}$
2004dk	17^{+4}_{-3}	$2.1^{0.5}_{-0.4}$	$0.23^{+0.14}_{-0.09}$
2004dn	13^{+3}_{-2}	$1.6^{+0.4}_{-0.3}$	$0.16^{+0.11}_{-0.06}$
2004fe	10^{+2}_{-2}	$1.3^{+0.3}_{-0.2}$	$0.19^{+0.11}_{-0.07}$
2004ff	10^{+4}_{-3}	$1.2^{+0.5}_{-0.3}$	$0.18^{+0.13}_{-0.08}$
2004ge	14^{+9}_{-4}	$1.8^{+1.1}_{-0.5}$	$0.59^{+0.44}_{-0.25}$
2004gq	13^{+6}_{-3}	$1.7^{+0.7}_{-0.4}$	$0.13^{+0.13}_{-0.07}$
2005az	18^{+9}_{-5}	$2.2^{+1.1}_{-0.6}$	$0.31^{+0.21}_{-0.13}$
2005eo	11^{+5}_{-3}	$1.4^{+0.6}_{-0.4}$	$0.33^{+0.33}_{-0.17}$
2005hg	13^{+3}_{-2}	$1.6^{+0.4}_{-0.3}$	$0.64^{+0.41}_{-0.26}$
2005kz	18^{+12}_{-6}	$2.2^{+1.5}_{-0.8}$	$0.47^{+0.31}_{-0.19}$
2006F	11^{+4}_{-3}	$1.4^{+0.6}_{-0.4}$	$0.21^{+0.17}_{-0.10}$
2006ab	14^{+6}_{-3}	$1.8^{+0.8}_{-0.4}$	$0.23^{+0.20}_{-0.11}$
2006dn	17^{+10}_{-5}	$2.1^{+1.3}_{-0.7}$	$0.30^{+0.44}_{-0.17}$
2006el	14^{+7}_{-4}	$1.7^{+0.9}_{-0.5}$	$0.13^{+0.11}_{-0.06}$
2007C	11^{+2}_{-2}	$1.4^{+0.3}_{-0.2}$	$0.16^{+0.12}_{-0.07}$
2007D	12^{+7}_{-4}	$1.5^{+0.8}_{-0.5}$	$1.5^{+0.5}_{-0.5}$
2007Y[a]	11^{+1}_{-1}	$1.4^{+0.1}_{-0.1}$	$\lesssim 0.05$
2007gr	10^{+2}_{-2}	$1.2^{+0.2}_{-0.2}$	$0.07^{+0.01}_{-0.01}$
2007ru	15^{+2}_{-1}	$1.9^{+0.2}_{-0.2}$	$0.45^{+0.08}_{-0.07}$
2008D	$14^{+0.3}_{-0.2}$	$1.8^{+0.4}_{-0.3}$	$0.07^{+0.02}_{-0.02}$
2008ax	10^{+1}_{-1}	$1.3^{+0.1}_{-0.1}$	$0.05^{0.02}_{-0.03}$

Note. [a] The properties observed for SN 2007Y reside at the edge of our model parameter grid, so our derived physical parameters are uncertain; we quote an upper limit for M_{Ni}.

6.2. Light Curve Widths

We next extract τ_c estimates for each SN in our extended sample and find similar average values for the sub-types of $\langle \tau_c \rangle = 13 \pm 3$ days (Type Ib), $\langle \tau_c \rangle = 12 \pm 4$ days (Type Ic), and $\langle \tau_c \rangle = 14 \pm 3$ days (Type Ic-BL; see Table 7). A K-S test on the sample τ_c values suggests a 90% probability that SNe Ib, Ic, and Ic-BL are drawn from the same parent population of explosions. For the engine-driven explosions, we find a similar average value of $\langle \tau_c \rangle = 12 \pm 3$ days. Thus, light curve width and/or early decline rate cannot be used to distinguish He-rich from He-poor events, nor does it serve as a proxy for which SNe Ic-BL harbor central engines. At the same time, the large dispersion in light curve widths points to a significant variation in the M_{ej} values and, in turn, the progenitor mass.

6.3. Estimates for M_{ej} and E_K

With reasonable assumptions for the average photospheric velocities of SNe Ib, Ic, and Ic-BL, we may break the degeneracy between M_{ej} and E_K implied by our mean τ_c estimates derived from our Δm_{15} measurements. Within the framework of the analytic light curve models, these two physical parameters

Table 7
Sample Averages

SN Type	$M_{V_{peak}}$ (mag)	$M_{R_{peak}}$ (mag)	M_{Ni} ($M_{\odot}$)	τ_c (days)	$M_{ej}^{3/4} E_K^{-1/4}$ ((10^{51} erg)$^{-1/4}$($M_{\odot}$)$^{3/4}$)	M_{ej}[a] ($M_{\odot}$)	E_K[a] (10^{51} erg)
SNe Ib	-17.6 ± 0.9	-17.9 ± 0.9	0.20 ± 0.16	13 ± 3	1.7 ± 0.3	$2.0^{+1.1}_{-0.8}$	$1.2^{+0.7}_{-0.5}$
SNe Ic	-18.0 ± 0.5	-18.3 ± 0.6	0.24 ± 0.15	12 ± 4	1.5 ± 0.4	$1.7^{+1.4}_{-0.9}$	$1.0^{+0.9}_{-0.5}$
SNe Ic-BL	-18.3 ± 0.8	-19.0 ± 1.1	0.58 ± 0.55	14 ± 3	1.7 ± 0.4	$4.7^{+2.3}_{-1.8}$	11^{+6}_{-4}
Engine-driven SNe	-18.9 ± 0.3	-18.9 ± 0.4	0.40 ± 0.18	12 ± 3	1.5 ± 0.3	$3.6^{+2.0}_{-1.6}$	$9.0^{+5.0}_{-4.0}$

Note. [a] Typical photospheric velocities of $v_{ph} = 10,000 \, \mathrm{km \, s^{-1}}$ are assumed for SNe Ib and Ic and $v_{ph} = 20,000 \, \mathrm{km \, s^{-1}}$ for SNe Ic-BL and engine-driven SNe.
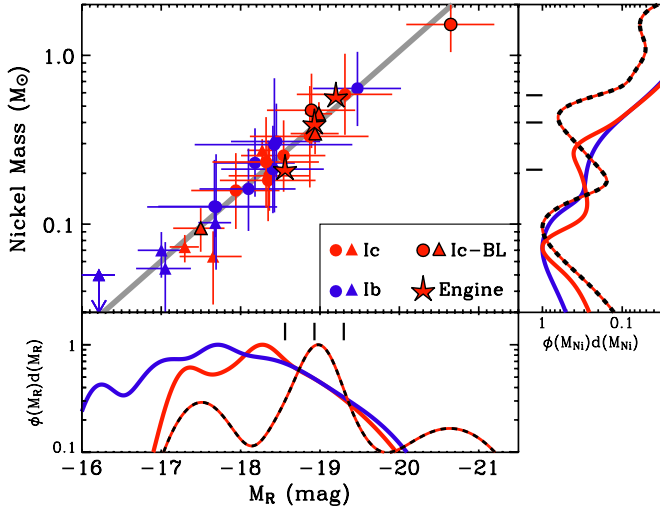
Figure 23. Model-derived Nickel-56 mass, M_{Ni}, and peak absolute magnitude, M_R, are compared for SNe Ib (blue), Ic (red) and broad-lined Ic (red encircled black) for the literature (triangles) and P60 (circles) samples. Engine-driven SNe Ic-BL are highlighted by stars. A clear trend is seen with an observed scatter due to the diversity in light curve widths. We find a best fit for the function, $\log(M_{Ni}) \approx -0.41 \, M_R - 8.3$ (gray solid line). The distributions of M_R and M_{Ni} are shown on the bottom and side panels, respectively, with engine-driven explosions shown by tick marks. SNe Ic-BL are more luminous and synthesize more Nickel-56 than SNe Ib and ordinary SNe Ic. Engine-driven explosions are statistically consistent with the SNe Ic-BL population.

(A color version of this figure is available in the online journal.)

depend on v_{ph} as follows:

$$M_{ej} \approx 0.8 \left(\frac{\tau_c}{8d} \right)^2 \left(\frac{v_{ph}}{10,000 \, \mathrm{km \, s^{-1}}} \right) M_{\odot}, \qquad (1)$$

$$E_{K,51} \approx 0.5 \left(\frac{\tau_c}{8d} \right)^2 \left(\frac{v_{ph}}{10,000 \, \mathrm{km \, s^{-1}}} \right)^3 \mathrm{erg.} \qquad (2)$$

For SNe Ib and Ic, we adopt $v_{ph} \approx 10,000 \, \mathrm{km \, s^{-1}}$ at maximum light, in line with spectroscopic observations (Matheson et al. 2001). For SNe Ic-BL and engine-driven SNe, the observed range of v_{ph} values is broader; we adopt $v_{ph} = 20,000 \, \mathrm{km \, s^{-1}}$ for the SNe Ic-BL at maximum light (e.g., Pian et al. 2006). Combining these assumptions with our average τ_c estimates for the combined sample (Table 6), we find typical values of $M_{ej} \approx 2 \, M_{\odot}$ and $E_{K,51} \approx 1$ erg for SNe Ib and Ic, while for SNe Ic-BL we find higher values, $M_{ej} \approx 5 \, M_{\odot}$ and $E_{K,51} \approx 10$ erg (Figure 24). For the three local engine-driven explosions, we estimate $M_{ej} \approx 4 \, M_{\odot}$ and $E_{K,51} \approx 9$ erg (Table 7). Thus, based on these reasonable estimates of v_{ph}, we find no evidence for different explosion parameters among SNe Ib and Ic, while those of SNe Ic-BL are distinct and more closely resemble the values inferred for engine-driven explosions.
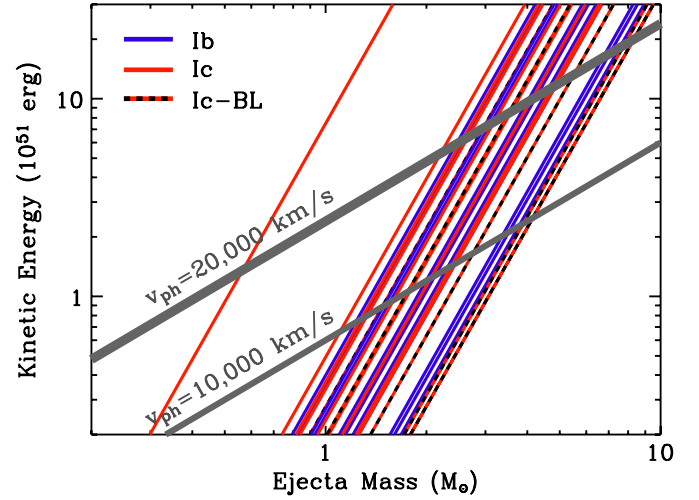

Figure 24. Our light curve modeling for each of the SNe Ib (blue), Ic (red), and Ic-BL (red/black) in our extended sample results in a degenerate solution for M_{ej} and E_K. Making reasonable assumptions for the photospheric velocities, v_{ph}, breaks this degeneracy. We assume that SNe Ibc have $v_{ph} = 10,000 \, \mathrm{km \, s^{-1}}$ and SNe Ic-BL have $v_{ph} = 20,000 \, \mathrm{km \, s^{-1}}$ at the epoch of maximum light (gray lines). The intersection point of the v_{ph} lines with each of the degenerate modeling solutions represents the implied physical parameters. We find average values of $M_{ej} \approx 2 \, M_{\odot}$ and $E_{K,51} \approx 1$ erg for SNe Ib and Ic while SNe Ic-BL show more extreme parameters: $M_{ej} \approx 5 \, M_{\odot}$ and $E_{K,51} \approx 10$ erg.

(A color version of this figure is available in the online journal.)

7. IMPLICATIONS FOR SNe Ibc PROGENITORS

Here we consider the implications for the progenitors of SNe Ibc based on their derived explosion parameters together with host galaxy and/or explosion site diagnostics. While we derive *similar* explosion properties for SNe Ib and Ic, their explosion site properties imply statistically significant *dissimilarities*. SNe Ic favor the more luminous and metal-rich regions of their host galaxies than SNe Ib (Kelly et al. 2008; Modjaz et al. 2011 but see Anderson et al. 2010). These explosion site diagnostics suggest that SNe Ic progenitors are more massive and/or younger and characterized by a slightly higher metal content than the progenitors of SNe Ib. More massive progenitors may produce explosions with larger M_{ej} values unless they are able to lose mass more efficiently throughout. Since the line-driven winds of Wolf-Rayet stars are enhanced at higher metallicity ($\dot{M} \propto Z^{0.8}$; Vink & de Koter 2005), we speculate that SNe Ic progenitors are initially more massive than those of SNe Ib but lose mass more efficiently, resulting in explosion parameters that appear indistinguishable from their helium-rich cousins.

Next, we consider the more extreme explosion parameters we infer for SNe Ic-BL in comparison to those of SNe Ibc. Explosion site metallicities for SNe Ic-BL do not reveal strong dissimilarities from those of SNe Ib and Ic (Anderson et al.

2010; Modjaz et al. 2011 but see Arcavi et al. 2010). However, a study of the explosion site luminosities indicates that SNe Ic-BL trace the star-forming light of their host galaxies at least as tightly as SNe Ic and perhaps as tightly as GRB-SNe (Kelly et al. 2008). At the same time, the light curves of SNe Ic-BL show evidence for more powerful explosions, with somewhat larger M_{ej} values than ordinary SNe Ibc (Table 7). We therefore speculate that SNe Ic-BL may represent the explosion of more massive progenitor stars than other SNe Ibc across a broad range of metallicities. This may also explain the existence of broad-lined SNe of Types Ib and IIb that stem from metal-poor progenitors (e.g., SN 2003bg; Hamuy et al. 2009).

Finally, we consider the relation of engine-driven SN progenitors with those of SNe Ic-BL. Based on their optical properties (light curves and spectra), SNe Ic-BL and engine-driven SNe appear statistically indistinguishable; however, radio observations reveal relativistic outflows in only a small fraction (Soderberg et al. 2010). Meanwhile, explosion site metallicity measurements indicate that engine-driven explosions tend to populate the low end of the metallicity distribution for SNe Ibc (Modjaz et al. 2011), although there are some notable exceptions (see Levesque et al. 2010). In these cases, an additional key parameter may be at play and possibly related to the rotation, binarity, or the nature of the compact remnant of the progenitor system (black hole, neutron star, or magnetar; Yoon et al. 2010).

8. CONCLUSIONS

We present the first uniform and statistical sample of SNe Ibc multi-band light curves available to date. We find a significant dispersion among the light curves both in peak luminosity and decay rate. Through a comparison with the existing small sample of well-observed SNe Ibc light curves from the literature, we find that a significant fraction of SNe Ibc are heavily extinguished with $E(B-V)_{host} \approx 0.4$ mag. After correcting our light curves for host galaxy extinction, we compare differential and cumulative distributions for the peak absolute magnitudes of SNe Ib, Ic, and Ic-BL. We find that the peak luminosity distributions for SNe Ib and Ic are statistically indistinguishable, with $\langle M_{R,peak} \rangle \approx -18$ mag and are therefore not inconsistent with a single progenitor channel for helium-poor and helium-rich events. A comparison of their early decline rates supports this hypothesis and we note there is no evidence for a correlation with peak absolute magnitude as is seen for SNe Ia. However, we find that SNe Ic-BL are typically more luminous with $\langle M_R \rangle \approx -19$ mag. The probability that they belong to the same set of progenitors and/or explosions as ordinary SNe Ib and Ic is just 2%.

We compare these observed light curve properties with those of the three nearby engine-driven SNe discovered within the same volume and find a significant overlap with the SNe Ic-BL population. The probability that engine-driven SNe are drawn from the SNe Ic-BL population is 25%, based on these optical diagnostics alone. This result underscores the point that neither high luminosity nor fast photospheric velocity can be used as a robust indicator for an engine-driven explosion, and thus radio searches for a relativistic outflow are required to distinguish (e.g., Soderberg et al. 2010).

We model the optical light curves in a systematic fashion to extract estimates of the three physical parameters, M_{Ni}, M_{ej}, and E_K, and find that the results reiterate those reviewed above. For example, there is no significant difference between SNe Ib and Ic and we estimate their physical parameters to be $M_{Ni} \approx 0.2\,M_{\odot}$, $M_{ej} \approx 2\,M_{\odot}$, and $E_{K,51} \approx 1$ erg. Meanwhile, SNe Ic-BL and

engine-driven events are similar to one another and distinct from ordinary SNe Ib and Ic; for them we estimate more extreme physical parameters of $M_{Ni} \approx 0.5\,M_{\odot}$, $M_{ej} \approx 5\,M_{\odot}$, and $E_{K,51} \approx 10$ erg. The statistically significant difference between ordinary SNe Ibc and SNe Ic-BL (including engine-driven events) suggests that the latter share a distinct ^{56}Ni production mechanism and/or ejecta distribution (e.g., bipolar outflow).

Looking forward, the inclusion of spectroscopic diagnostics (e.g., v_{ph} measurements, and He I feature intensities) would enable an extension of this systematic study to search for additional correlations and to properly break the model degeneracies between M_{ej} and E_K. Along this line, we reiterate that 10 of the SNe in our study were observed as part of the CCCP and thus spectroscopic observations (often extensive) exist for this subsample. This project will be the focus of a separate study. Furthermore, a direct comparison of host galaxy diagnostics with optical light curve properties (e.g., peak luminosity) may reveal further clues on the nature of SN Ibc progenitors and their relation to those of engine-driven explosions. Since our sample is drawn from targeted surveys, it is likely biased toward metal-rich host galaxies. Fortunately, new wide-field transient surveys such as Pan-STARRS (Kaiser et al. 2002) and the Palomar Transient Factory (Law et al. 2009) are discovering SNe in a broad range of host galaxy environments and will enable such comparisons to be made in an unbiased fashion. Moreover, thanks to the higher cadence of these optical surveys, SNe Ibc will be discovered earlier with respect to the explosion date, reducing the fraction of Bronze SNe in future follow-up samples. Finally, we note that the significant $E(B-V)_{host}$ values inferred here motivate the regular use of near-IR facilities in future studies of SNe Ibc.

REFERENCES

Aldering, G., Lee, B. C., Loken, S., et al. 2005, ATel, 451, 1
Anderson, J. P., Covarrubias, R. A., James, P. A., Hamuy, M., & Habergham, S. M. 2010, MNRAS, 407, 2660
Antilogus, P., Gilles, S., Pain, R., et al. 2006, ATel, 854, 1
Arcavi, I., Gal-Yam, A., Kasliwal, M. M., et al. 2010, ApJ, 721, 777
Arnett, W. D. 1982, ApJ, 253, 785
Baek, M., Li, W., Puckett, T., Sostero, G., & Garzia, S. 2006, IAU Circ., 8660, 1
Begelman, M. C., & Sarazin, C. L. 1986, ApJ, 302, L59
Berger, E., Kulkarni, S. R., Frail, D. A., & Soderberg, A. M. 2003, ApJ, 599, 408
Blondin, S., Modjaz, M., Kirshner, R., Challis, P., & Calkins, M. 2006, CBET, 626, 1
Blondin, S., Prieto, J. L., Patat, F., et al. 2009, ApJ, 693, 207
Cano, Z., Bersier, D., Guidorzi, C., et al. 2011, arXiv:1104.5141
Cenko, S. B., Fox, D. B., Moon, D.-S., et al. 2006, PASP, 118, 1396
Chevalier, R. A. 1998, ApJ, 499, 810

Chevalier, R. A., & Fransson, C. 2006, ApJ, 651, 381
Chevalier, R. A., & Soderberg, A. M. 2010, ApJ, 711, L40
Clocchiatti, A., & Wheeler, J. C. 1997a, ApJ, 491, 375
Clocchiatti, A., & Wheeler, J. C. 1997b, arXiv:astro-ph/9601023
Clocchiatti, A., Wheeler, J. C., Benetti, S., & Frueh, M. 1996, ApJ, 459, 547
Colesanti, C., Jacques, C., Pimentel, E., et al. 2006a, IAU Circ., 8658, 2
Colesanti, C., Jacques, C., Pimentel, E., et al. 2006b, IAU Circ., 8713, 1
Conley, A., Howell, D. A., Howes, A., et al. 2006, AJ, 132, 1707
de Vaucouleurs, G., de Vaucouleurs, A., Corwin, Jr. H. G., et al. 1991, Third Reference Catalogue of Bright Galaxies (New York: Springer)
Elias, J. H., Matthews, K., Neugebauer, G., & Persson, S. E. 1985, ApJ, 296, 379
Filippenko, A. V. 1997, ARA&A, 35, 309
Filippenko, A. V., & Foley, R. J. 2004, IAU Circ., 8453, 3
Filippenko, A. V., Foley, R. J., & Matheson, T. 2005, IAU Circ., 8639, 2
Filippenko, A. V., Ganeshalingam, M., Serduke, F. J. D., & Hoffman, J. L. 2004, IAU Circ., 8404, 1
Filippenko, A. V., & Sargent, W. L. W. 1985, Nature, 316, 407
Folatelli, G., Contreras, C., Phillips, M. M., et al. 2006, ApJ, 641, 1039
Foley, R. J., & Gal-Yam, A. 2007, CBET, 805, 1
Foley, R. J., Papenkova, M. S., Swift, B. J., et al. 2003, PASP, 115, 1220
Foley, R. J., Smith, N., Ganeshalingam, M., et al. 2007, ApJ, 657, L105
Gal-Yam, A., Cenko, S. B., Fox, D. B., et al. 2007, in AIP Conf. Ser. 924, The Multicolored Landscape of Compact Objects and Their Explosive Origins, ed. T. di Salvo, G. L. Israel, L. Piersant, L. Burderi, G. Matt, A. Tornambe, & M. T. Menna (New York: AIP), 297
Gal-Yam, A., Fox, D. B., Kulkarni, S. R., et al. 2005, ApJ, 630, L29
Gal-Yam, A., Mazzali, P., Ofek, E. O., et al. 2009, Nature, 462, 624
Galama, T. J., Vreeswijk, P. M., van Paradijs, J., et al. 1998, Nature, 395, 670
Ganeshalingam, M., Swift, B. J., Serduke, F. J. D., & Filippenko, A. V. 2004, IAU Circ., 8456, 4
Graham, J., & Li, W. 2004a, IAU Circ., 8377, 2
Graham, J., & Li, W. 2004b, IAU Circ., 8381, 1
Greiner, J., et al. 2010, in AIP Conf. Ser. 1279, Deciphering the Ancient Universe with Gamma-ray Bursts, ed. N. Kawai & S. Nagataki (New York: AIP), 144
Hamuy, M., Deng, J., Mazzali, P. A., et al. 2009, ApJ, 703, 1612
Hamuy, M., Maza, J., Pinto, P. A., et al. 2002, AJ, 124, 417
Hayden, B. T., Garnavich, P. M., Kessler, R., et al. 2010, ApJ, 712, 350
Hubble, E. P. 1926, ApJ, 64, 321
Hunter, D. J., Valenti, S., Kotak, R., et al. 2009, A&A, 508, 371
Itagaki, K., Nakano, S., Puckett, T., et al. 2006, IAU Circ., 8762, 1
Iwamoto, K., Mazzali, P. A., Nomoto, K., et al. 1998, Nature, 395, 672
Iwamoto, K., Nomoto, K., Mazzali, P. A., et al. 2003, in Lecture Notes in Physics 598, Supernovae and Gamma-ray Bursters, ed. K. Weiler (Berlin: Springer), 243
Joubert, N., Li, W., Puckett, T., et al. 2007, IAU Circ., 8794, 3
Kaiser, N., Aussel, H., Burke, B. E., et al. 2002, Proc. SPIE, 4836, 154
Kelly, P. L., Kirshner, R. P., & Pahre, M. 2008, ApJ, 687, 1201
Law, N. M., Kulkarni, S. R., Dekany, R. G., et al. 2009, PASP, 121, 1395
Lee, E., Baek, M., & Li, W. 2006, IAU Circ., 8669, 1
Levesque, E. M., Soderberg, A. M., Foley, R. J., et al. 2010, ApJ, 709, L26
Li, W., Leaman, J., Chornock, R., et al. 2011, MNRAS, 412, 1441
MacFadyen, A. I., Woosley, S. E., & Heger, A. 2001, ApJ, 550, 410
Matheson, T., Filippenko, A. V., Li, W., Leonard, D. C., & Shields, J. C. 2001, AJ, 121, 1648
Mazzali, P. A., Deng, J., Nomoto, K., et al. 2006, Nature, 442, 1018
Mazzali, P. A., Kawabata, K. S., Maeda, K., et al. 2007a, ApJ, 670, 592
Mazzali, P. A., Röpke, F. K., Benetti, S., & Hillebrandt, W. 2007b, Science, 315, 825
Mirabal, N., Halpern, J. P., An, D., Thorstensen, J. R., & Terndrup, D. M. 2006, ApJ, 643, L99
Modjaz, M., Blondin, S., Kirshner, R., et al. 2006, CBET, 677, 1
Modjaz, M., Bloom, J. S., Filippenko, A. V., et al. 2011, ApJ, 731, 4
Modjaz, M., Challis, P., Kirshner, R., Matheson, T., & Berlind, P. 2005a, IAU Circ., 8605, 2
Modjaz, M., Challis, P., Kirshner, R., et al. 2004a, IAU Circ., 8428, 3
Modjaz, M., Challis, P., Kirshner, R., et al. 2004b, IAU Circ., 8426, 3
Modjaz, M., Kirshner, R., Challis, P., Blondin, S., & Berlind, P. 2005b, IAU Circ., 8650, 2
Modjaz, M., Kirshner, R., Challis, P., Matheson, T., & Berlind, P. 2005c, CBET, 271, 1
Modjaz, M., Kirshner, R., Challis, P., et al. 2005d, IAU Circ., 8461, 2
Monard, L. A. G., Quimby, R., Gerardy, C., et al. 2004, IAU Circ., 8454, 1
Moore, M., Shimasaki, K., & Li, W. 2004, IAU Circ., 8443, 3
Mould, J. R., Huchra, J. P., Freedman, W. L., et al. 2000, ApJ, 529, 786

Munari, U., & Zwitter, T. 1997, A&A, 318, 269
Newton, J., & Puckett, T. 2005, IAU Circ., 8648, 2
Nomoto, K., Maeda, K., Mochizuki, Y., et al. 2001, in AIP Conf. Ser. 587, Gamma 2001: Gamma-Ray Astrophysics, ed. S. Ritz, N. Gehrels, & C. R. Shrader (New York: AIP), 487
Nomoto, K., Tominaga, N., Umeda, H., Kobayashi, C., & Maeda, K. 2006, Nucl. Phys. A, 777, 424
Pastorello, A., Kasliwal, M. M., Crockett, R. M., et al. 2008a, MNRAS, 389, 955
Pastorello, A., Quimby, R. M., Smartt, S. J., et al. 2008b, MNRAS, 389, 131
Pastorello, A., Smartt, S. J., Mattila, S., et al. 2007, Nature, 447, 829
Perets, H. B., Gal-Yam, A., Mazzali, P. A., et al. 2010, Nature, 465, 322
Perley, D. A., Cenko, S. B., Bloom, J. S., et al. 2009, AJ, 138, 1690
Phillips, M. M. 1993, ApJ, 413, L105
Phillips, M. M., Lira, P., Suntzeff, N. B., et al. 1999, AJ, 118, 1766
Pian, E., Amati, L., Antonelli, L. A., et al. 2000, ApJ, 536, 778
Pian, E., Mazzali, P. A., Masetti, N., et al. 2006, Nature, 442, 1011
Pignata, G., Stritzinger, M., Soderberg, A, et al. 2011, ApJ, 728, 14
Podsiadlowski, P., Joss, P. C., & Hsu, J. J. L. 1992, ApJ, 391, 246
Podsiadlowski, P., Mazzali, P. A., Nomoto, K., Lazzati, D., & Cappellaro, E. 2004, ApJ, 607, L17
Porter, A. C., & Filippenko, A. V. 1987, AJ, 93, 1372
Prasad, R. R., Joubert, N., Baek, M., et al. 2006, IAU Circ., 8770, 1
Prieto, J. L., Stanek, K. Z., & Beacom, J. F. 2008, ApJ, 673, 999
Puckett, T., Gagliano, R., Mostardi, R., et al. 2006a, IAU Circ., 8750, 2
Puckett, T., Orff, T., Madison, D., et al. 2007, IAU Circ., 8792, 2
Puckett, T., Peoples, M., Joubert, N., et al. 2006b, IAU Circ., 8741, 1
Puckett, T., Peoples, M., Prasad, R. R., et al. 2005a, IAU Circ., 8605, 1
Puckett, T., Sostero, G., Quimby, R., & Mondol, P. 2005b, IAU Circ., 8639, 1
Pugh, H., Li, W., Manzini, F., & Behrend, R. 2004, IAU Circ., 8452, 2
Pugh, H., Park, S., & Li, W. 2004, IAU Circ., 8425, 1
Quimby, R., Gerardy, C., Hoeflich, P., et al. 2004, IAU Circ., 8446, 1
Quimby, R. M., Kulkarni, S. R., Kasliwal, M. M., et al. 2011, Nature, 474, 487
Quimby, R., Mondol, P., Castro, F., Roman, B., & Rostopchin, S. 2006, IAU Circ., 8657, 1
Quimby, R., Mondol, P., Hoeflich, P., Wheeler, J. C., & Gerardy, C. 2005, IAU Circ., 8503, 1
Richardson, D. 2009, AJ, 137, 347
Richardson, D., Branch, D., & Baron, E. 2006, AJ, 131, 2233
Richmond, M. W., van Dyk, S. D., Ho, W., et al. 1996, AJ, 111, 327
Riess, A. G., Filippenko, A. V., Li, W., et al. 1999, AJ, 118, 2675
Sahu, D. K., Tanaka, M., Anupama, G. C., Gurugubelli, U. K., & Nomoto, K. 2009, ApJ, 697, 676
Saviane, I., Hibbard, J. E., & Rich, R. M. 2004, AJ, 127, 660
Schlegel, D. J., Finkbeiner, D. P., & Davis, M. 1998, ApJ, 500, 525
Schwehr, J., & Li, W. 2006, IAU Circ., 8728, 2
Shimasaki, K., & Li, W. 2005, IAU Circ., 8623, 2
Silbermann, N. A., Harding, P., Madore, B. F., et al. 1996, ApJ, 470, 1
Smartt, S. J. 2009, ARA&A, 47, 63
Smartt, S. J., Eldridge, J. J., Crockett, R. M., & Maund, J. R. 2009, MNRAS, 395, 1409
Smith, J. A., Tucker, D. L., Kent, S., et al. 2002, AJ, 123, 2121
Smith, N., Foley, R. J., & Filippenko, A. V. 2008, ApJ, 680, 568
Soderberg, A. M. 2007, PhD thesis, Caltech
Soderberg, A. M., Berger, E., Page, K. L., et al. 2008, Nature, 453, 469
Soderberg, A. M., Chakraborti, S., Pignata, G., et al. 2010, Nature, 463, 513
Soderberg, A. M., Kulkarni, S. R., Price, P. A., et al. 2006a, ApJ, 636, 391
Soderberg, A. M., Nakar, E., Berger, E., & Kulkarni, S. R. 2006b, ApJ, 638, 930
Stritzinger, M., Hamuy, M., Suntzeff, N. B., et al. 2002, AJ, 124, 2100
Stritzinger, M., Mazzali, P., Phillips, M. M., et al. 2009, ApJ, 696, 713
Takáts, K., & Vinkó, J. 2006, MNRAS, 372, 1735
Taubenberger, S., Pastorello, A., Mazzali, P. A., et al. 2006, MNRAS, 371, 1459
Thompson, T. A., Chang, P., & Quataert, E. 2004, ApJ, 611, 380
Uomoto, A., & Kirshner, R. P. 1985, A&A, 149, L7
Valenti, S., Benetti, S., Cappellaro, E., et al. 2008, MNRAS, 383, 1485
van Dyk, S. D., Hamuy, M., & Filippenko, A. V. 1996, AJ, 111, 2017
Vink, J. S., & de Koter, A. 2005, A&A, 442, 587
Weiler, K. W., Sramek, R. A., Panagia, N., van der Hulst, J. M., & Salvati, M. 1986, ApJ, 301, 790
Wheeler, J. C., & Levreault, R. 1985, ApJ, 294, L17
Wong, D. S., Silverman, J. M., Pooley, D., & Filippenko, A. V. 2006, IAU Circ., 8677, 3
Woosley, S. E., & Bloom, J. S. 2006, ARA&A, 44, 507
Woosley, S. E., Heger, A., & Weaver, T. A. 2002, Rev. Mod. Phys., 74, 1015
Woosley, S. E., Langer, N., & Weaver, T. A. 1995, ApJ, 448, 315
Yoon, S., Woosley, S. E., & Langer, N. 2010, ApJ, 725, 940

ERRATUM: "THE FIRST SYSTEMATIC STUDY OF TYPE Ibc SUPERNOVA MULTI-BAND LIGHT CURVES" (2011, ApJ, 741, 97)

Maria R. Drout[1,2], Alicia M. Soderberg[1], Avishay Gal-Yam[3], S. Bradley Cenko[4], Derek B. Fox[5],
Douglas C. Leonard[6], David J. Sand[7,8], Dae-Sik Moon[9], Iair Arcavi[3], and Yoav Green[3]

[1] Harvard-Smithsonian Center for Astrophysics, 60 Garden Street, MS-51 Cambridge, MA 02138, USA
[2] Churchill College, Cambridge CB3 0DS, UK
[3] Benoziyo Center for Astrophysics, Faculty of Physics, The Weizmann Institute of Science, Rehovot 76100, Israel
[4] Department of Astronomy, University of California, Berkeley, CA 94720-3411, USA
[5] Department of Astronomy and Astrophysics, Pennsylvania State University, 525 Davey Lab, University Park, PA 16802, USA
[6] Department of Astronomy, San Diego State University, San Diego, CA 92182, USA
[7] Las Cumbres Observatory Global Telescope Network, 6740 Cortona Drive, Suite 102, Santa Barbara, CA 93117, USA
[8] Department of Physics, Broida Hall, University of California, Santa Barbara, CA 93106, USA
[9] Department of Astronomy and Astrophysics, University of Toronto, Toronto, ON M5S 3H4, Canada
Received 2012 May 30; published 2012 June 26

Online-only material: machine-readable table

We report an error in the photometry for SN 2004dk in Table 2 of the published paper. In its originally published form, the table presents two copies of the SN 2004dk *R*-band photometry, rather than both the *V* and *R* bands. None of the results of the paper are changed as this error was simply typographical in nature. The correct photometry is given in Table 2, and a new machine-readable table is attached to this manuscript. We thank Justyn Maund for pointing out this discrepancy.

Table 2
P60 Photometry

SN	Filter	JD	Magnitude
SN 2004dk	*V*	2453219.8	17.32 ± 0.03
⋯	⋯	2453220.7	17.00 ± 0.03
⋯	⋯	2453223.8	16.12 ± 0.02
⋯	⋯	2453227.7	15.55 ± 0.02
⋯	⋯	2453233.7	15.01 ± 0.02
⋯	⋯	2453234.7	14.97 ± 0.02
⋯	⋯	2453235.7	14.94 ± 0.02
⋯	⋯	2453237.8	14.83 ± 0.02
⋯	⋯	2453242.7	14.88 ± 0.02
⋯	⋯	2453252.7	15.31 ± 0.02
⋯	⋯	2453258.6	15.54 ± 0.02
⋯	⋯	2453261.6	15.67 ± 0.02
⋯	⋯	2453270.7	15.95 ± 0.03

(This table is available in its entirety in a machine-readable form in the online journal. A portion is shown here for guidance regarding its form and content.)